 doi:10.20944/preprints201710.0166.v2

Données image et décision: détection automatique de variations dans des séries temporelles par réseau de Kohonen

Using the quantization error from Self-Organizing Map (SOM) output for fast detection of critical variations in image time series

Birgitta Dresp-Langley*, John Mwangi Wandeto+*, Henry Okola Nyongesa+

birgitta.dresp@icube.unistra.fr
john.wandeto@etu.unistra.fr
henry.nyongesa@gmail.com

** ICube Lab CNRS and University of Strasbourg, Strasbourg, France*
+Dedan Kimathi University of Technology, Nyeri, Kenya

E-mail for correspondence: birgitta.dresp@icube.unistra.fr

Keywords: Self-Organizing Map (SOM); quantization error; image time series; spatial contrast; variability; change detection

 doi:10.20944/preprints201710.0166.v2

Abstract

The quantization error (QE) from Self-Organizing Map (SOM) output after learning is exploited in this studies. SOM learning is applied on time series of spatial contrast images with variable relative amount of white and dark pixel contents, as in monochromatic medical images or satellite images. It is proven that the QE from the SOM output after learning provides a reliable indicator of potentially critical changes in images across time. The QE increases linearly with the variability in spatial contrast contents of images across time when contrast intensity is kept constant. The hitherto unsuspected capacity of this metric to capture even the smallest changes in large bodies of image time series after using ultra-fast SOM learning is illustrated on examples from SOM learning studies on computer generated images, MRI image time series, and satellite image time series. Linear trend analysis of the changes in QE as a function of the time an image of a given series was taken gives proof of the statistical reliability of this metric as an indicator of local change. It is shown that the QE is correlated with significant clinical, demographic, and environmental data from the same reference time period during which test image series were recorded. The findings show that the QE from SOM, which is easily implemented and requires computation times no longer than a few minutes for a given image series of 20 to 25, is useful for a fast analysis of whole series of image data when the goal is to provide an instant statistical decision relative to change/no change between images.

 doi:10.20944/preprints201710.0166.v2

Introduction

This work deals with a fast computational approach to change detection in complex images. The approach exploits the previously ignored potential of a change indicator, provided in the output data of the Self-Organizing Map (SOM), a well-documented computational analysis tool introduced many years ago by Teuvo Kohonen [1, 2]. SOM is a biologically inspired artificial neural network architecture that learns in an non-supervised way to detect spatial contrast variations in images. The artificial neurons possess some of the functional properties of visual neurons found in the mammalian cortex [3-6], such as sensitivity to spatial extent of contrast and contrast intensity in complex images. The architecture of SOM is relatively simple compared with other machine learning algorithms [1, 2], and the user decides about the number of neurons, and their selectivity to a given polarity of monochromatic contrast or colour.

The output of SOM is expressed in terms of the final synaptic weight of the neurons after learning, and their quantization error (QE), which is a measure of variance. It is this latter, the QE, that will be exploited here in this thesis to show that it constitutes a statistically reliable indicator of the smallest, potentially critical local change across images of a time series. SOM is easily implemented and the computation times for generating SOM output on large data sets with 20 or more images in a time series are ultra-fast, i.e. between 60 and 250 seconds for an image series.

After a general overview of SOM and its functional principles, we describe a series of proof-of-concept studies on computer generated images. On the basis of statistical regression analysis, it will be shown that the QE from the SOM output after learning displays a statistically significant sensitivity to systematic variations in the spatial extent of contrast in images of a series when the intensity of contrast is constant, and a statistically significant sensitivity to systematic variations in the intensity of contrast in the images when their spatial extent is constant. These results show that the QE from the SOM output reliably reflects two of the major functional characteristics of detection by natural visual systems as found in primates and other superior mammals. A vast body of literature from the neurosciences has shown that these functional properties are critical aspects of visual detection and analysis [7-16]. Simulations on random dot images with variations in the size of a single local dot are described, showing that the QE from the SOM output after learning consistently signals these very small changes.

On the basis of this body of proof of concept, it is postulated that the QE from the SOM output after learning provides a statistically reliable indicator of smallest and changes in image series that may be undetectable by human natural vision. It allows for the automatic detection of changes in the spatial extent of contrast across images, working on minimally preprocessed images to ensure that contrast intensity does not vary between images of a time series. This is applied here to series of medical (MRI) images [21-30] with small invisible local increases in lesion contents are submitted to SOM to show the usefulness of the QE approach for a fast processing of medical image data when the first problem to be addressed is to decide whether a clinically critical image contrast in a medical region of interest (mROI) relative to a lesion or a tumor is likely to have changed with time, either in the direction of local increase (the patient's condition is getting worse) or in the direction of local decrease (the patient's condition is getting better). Then, the QE approach is applied to extracts from time series of satellite images of the Nevada Desert and Las Vegas City, USA. The original images for a reference time period between 1984 and 2008 were taken from NASA's Landsat database and fed into minimal preprocessing to eliminate variations in contrast intensity. It will be shown that the QE from SOM output reliably reflects critical structural changes in the landscapes of specific geographic regions

Preprints (www.preprints.org) | NOT PEER-REVIEWED | Posted: 20 March 2018 doi:10.20944/preprints201710.0166.v2

of interest (gROI), such as Las Vegas City, the residential suburbia of Las Vegas in the North and the region of Lake Mead, which is an artificial reservoir enclosed by the Hoover Dam that collects water from the Colorado River, providing sustenance in water supply to the whole of Nevada and beyond [31]. While the originally monotonous desert landscapes of the gROI Las Vegas City and the residential North underwent major restructuration in the years of the reference time period from which the image time series were taken, resulting in the progressive increase in landscape variability due to man-mad building structures and developments, the landscape of the gROI Lake Mead became increasingly arid during the same time period, with water levels of Lake Mead progressively dwindling away over the years due to global climate change. These two opposite trends are reliably reflected by the corresponding variations in the QE from the SOM output after neural learning, for the different image time series corresponding to the different gROI. Linear trend analyses and correlation statistics are provided to further highlight important links between man-induced changes and demographic data [32] on the one hand, and between the natural phenomenon of drought and water level statistics from the Hoover Dam Control Room on the other.

The detection and characterization of critical changes in objects, event scenes, or public spaces of the natural or the built environment reflected by changes in image time series such as computer generated image data, photographs, medical images, or remotely sensed image data may be of considerable importance for swift decision making in various fields including the medical, human and environmental safety, policy making for risk mitigation, or public awareness campaigns. The context of emergency places a premium on fast automatic techniques for discriminating between changed and unchanged contents in large image time series, and computational methods of change detection in image data exploiting different types of transforms and algorithms have been developed previously by others [33-51] to meet this challenge. Existing methods have been reviewed previously in excellent papers by [33] and [34]. Known computations include Otsu's algorithm [35], Kapur's algorithm [36], and various other procedures such as pixel-based change detection, image differencing, automated thresholding, image rationing, regression analysis on image data, the least-square method for change detection, change vector analysis, median filtering, background filtering, and fuzzy logic algorithms [37-51]. The scope of any of these methods is limited by the specific goal pursued. In general terms, change detection consists of identifying differences in the state of an object or phenomenon by observing it at different times and implies being able to quantify change(s) due to the effect of time on that given object or phenomenon. In image change detection this involves being able to reveal critical changes through analysis of discrete data sets drawn from image time series. Major applications of change detection concern medical and remotely sensed data. Both are obtained by reliable methods of image acquisition to provide image time series through repetitive coverage at short intervals with consistent image quality, as shown previously [33, 51, 52].

The Self-Organizing Map (SOM)

The Self Organizing Map (SOM) is a neural network architecture [1, 2] inspired by the functional architecture of sensory neurons identified in the central nervous system (cortex) of mammals[3-6]. The neural learning procedure is unsupervised with specific self-organizing dynamics that do not require error correction as do supervised learning algorithms. SOM produces a lower-dimension representation of the input space and for each input vector, a competitive *winner-take-all* learning algorithm [1, 2] achieves the lower-dimension visualization of the input data. SOMs are typically applied as feature classifiers of input data starting from an initially random feature map. The input data are recursively fed into the learning procedure to optimize the final map into a stable

Preprints (www.preprints.org) | NOT PEER-REVIEWED | Posted: 20 March 2018 doi:10.20944/preprints201710.0166.v2

representation of features and regions of interest (ROI). Each region of the map can be considered in terms of a specific feature class of the input space. Whenever the synaptic weights associated with a node of the map match the input vector, that specific map area is selectively optimized to more closely resemble the data of the class the input vector belongs to. From an initial distribution of random weights, over thousands of iterations, SOM progressively sets up a map of stable representations of image regions or ROI. Each corresponding region of the final map is a feature classifier and one can think of the graphical output as a certain type of feature map of the input space.

1.1. SOM neural learning: winner takes all

The vector space of the SOM is by definition Euclidean [1, 2], and the central idea behind the principles of Self-Organizing mapping is that every input data item shall be matched to the closest fitting neuron of the neural map, called the winner (as denoted by M_c in Figure 1). The winning neurons for the corresponding regions are progressively modified on that principle until they optimally match the entire data set. The learning procedure follows the neurobiological principles of *lateral inhibition* [53] and the general rule of *Hebbian* synaptic learning [54]. On the other hand, since the spatial neighbourhood around the winners in the map is continuously modified during learning, a degree of local and differential ordering of the map is mathematically applied. This principle is called *smoothing.* The resulting local ordering effects will gradually be propagated across the entire SOM. The parameters in SOM models can be variable and depend on the type of learning algorithm implemented. The final goal of winner-take-all learning is to ensure that the final map output after learning stably represents critical similarities in the input data.

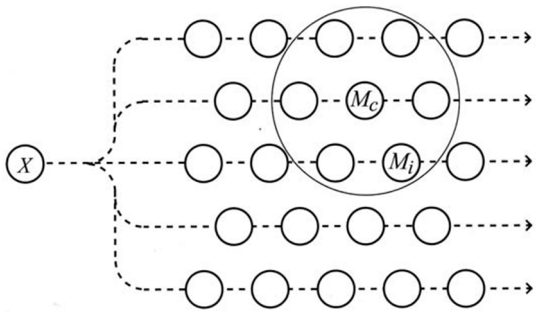

Figure 1. Illustration of a self-organizing map (after Kohonen [1, 2]). An input data item X is broadcast to a set of model nodes M_i , of which M_c matches X best . All models that lie in the neighbourhood (larger circle) of M_c in the network match X better than others at further away locations.

1.2. Network dynamics

The adaptation of the synaptic vectors in our method here is done as earlier proposed by Kohonen himself [1, 2]:

1. Determine the best-matching unit for the current input signal.
2. Increase matching at the best-matching unit and its topologically nearest neighbours.

In Kohonen's model the strength of the adaptation is decreasing according to a cooling

Preprints (www.preprints.org) | NOT PEER-REVIEWED | Posted: 20 March 2018 doi:10.20944/preprints201710.0166.v2

schedule. Moreover, the topological neighbourhood inside which significant changes are made is chosen large at the beginning and decreases then, too. Our SOM approach here follows the same basic strategy. There are, however, two important differences:

1. The adaptation strength is constant over time. Specifically, we use constant adaptation parameters for the best-matching unit and the neighbouring neurons.
2. Only the best-matching unit and its direct topological neighbours are adapted. These choices eliminate the need to define a cooling schedule for any of the SOM parameters.

1.3. SOM output: final synaptic weights

As becomes clear in the light of what is summarized above, the SOM as approached here can be seen as a statistical method of data analysis using an unsupervised learning algorithm (some have combined SOM with supervised learning algorithms, which does not apply to this work here and will not be discussed as it is beyond the scope of this thesis) whose goal is to determine relevant properties of input data without explicit feedback from a teacher. Originally inspired by feature maps in sensory systems, it has greatly contributed to our understanding of principles of self-organization in the brain and the development of feature maps. Through an interplay of neural principles of *lateral inhibition* and *Hebbian* synaptic learning within a localized region of a one-layered neural network, the SOM acquires a low-dimensional representation of high-dimensional input features (x) that respects topological relationships of the input space. This is progressively achieved through the updating of the synaptic weights (wj) of winning units at iterations (i) over time (t) during learning:

$$\Delta wij(t) = \alpha(t) * (xi(t) - wij(t) \qquad (1)$$

where α is the fixed learning rate. At the end of learning, when all neurons optimally match the data from the learned set, SOM generates two types of output data: the matrix of the final synaptic weights of neurons and their quantization error (QE).

1.4. SOM output: the quantization error (QE)

As an output of SOM associated with the final synaptic weights of neurons after learning, the quantization error (QE) is a statistical measure of variance. It has sometimes been used to evaluate the quality of SOMs, or to benchmark a series of SOMs with different parameters trained on one and the same dataset [1, 2, 27, 28]. In this thesis, we exploit the QE to a different and entirely novel purpose. The goal here is to benchmark a series of learnt datasets using a SOM with the same parameters. In other words, we use the same SOM, same map size, feature size, learning rate and neighborhood radius to analyze series of image datasets with clinical significance, or random-dot images, as shown later herein. The QE is obtained from the SOM output after learning and mathematically expresses the squared distance (usually the average Euclidean distance) between input data x and their corresponding so-called *best matching units* (BMU). Thus, the QE reflects the average distance between each data vector (X) and its BMU:

$$QE = 1/N \sum_{i=1}^{N} \left\| X_i - \left(BMU_{(i)} \right) \right\| \qquad (2)$$

where N is the number of sample vectors x in the input data.

Preprints (www.preprints.org) | NOT PEER-REVIEWED | Posted: 20 March 2018 doi:10.20944/preprints201710.0166.v2

The QE is a statistical measure of variance associated with the final synaptic weights of the SOM output after learning. It disregards map topology and alignment [28] and its calculation, like that of the final synaptic weights, results directly from the unsupervised learning procedure. On this basis, it is postulated that the QE reflects critical variations in the *map-to-data matching* process in a similar way as the statistical variance around a mean reflects the dispersion of the raw data around that mean. As for one and the same mean we can have differently dispersed raw data, we can have differently dispersed *Euclidean* distances between map nodes and the raw input data for one and the same final synaptic weight after learning.

1.4. Hypothesis: the QE reflects critical spatial variations in image contrast

In the case of image data for one and the same object, variations in the QE output from SOM could be due to small local differences in the distribution of spatial contrast across images of a time series. This possibility has been as far as we know not been explored before, yet, it opens new possibilities for the fast automatic processing of series of image data for which a quick decision about change or no change needs to be made. To provide the necessary proof of concept that validates the postulate here above, a series of test simulations on times series of computer generated images was performed to give proof that:

1. The QE from the SOM output after learning is sensitive in a statistically significant measure to the spatial extent of variation in local contrast regions across images when the intensity of contrast is constant.

2. The QE from the SOM output after learning is sensitive in a statistically significant measure to differences in the intensity of local contrast regions across images when the spatial extent of contrast is constant.

2. Proof of concept

The goal of the following proof-of-concept study is to show that the QE varies consistently, reliably, and predictably with local variations in spatially distributed contrast signals in random-dot images, and in image series with regularly distributed spatial contrasts (geometric configurations). On the grounds of these systematic variations, it will be shown that the QE is a highly sensitive and reliable indicator of local and global image homogeneity: as images from a time series become more heterogeneous in spatial contents, the QE in the SOM output after learning consistently increases; conversely, as images from a time series become more homogenous in spatial contents, the QE consistently decreases, provided the intensity of contrast is constant across images of a given series.

2.1. Materials and methods

All images generated for the study had the same size in terms of x, y screen pixel coordinates (792 x 777 pixels). Time series of images with variable amount of black and white pixel contents were generated. In a given time series, the percentage of spatially distributed white and black pixel contents was increased systematically, the contrast intensity was kept constant within and across image series. In the last series, the opposite case where spatial extent of contrast is constant, but contrast intensity varies across images of a series is tested to finalize the proof of concept.

Preprints (www.preprints.org) | NOT PEER-REVIEWED | Posted: 20 March 2018 doi:10.20944/preprints201710.0166.v2

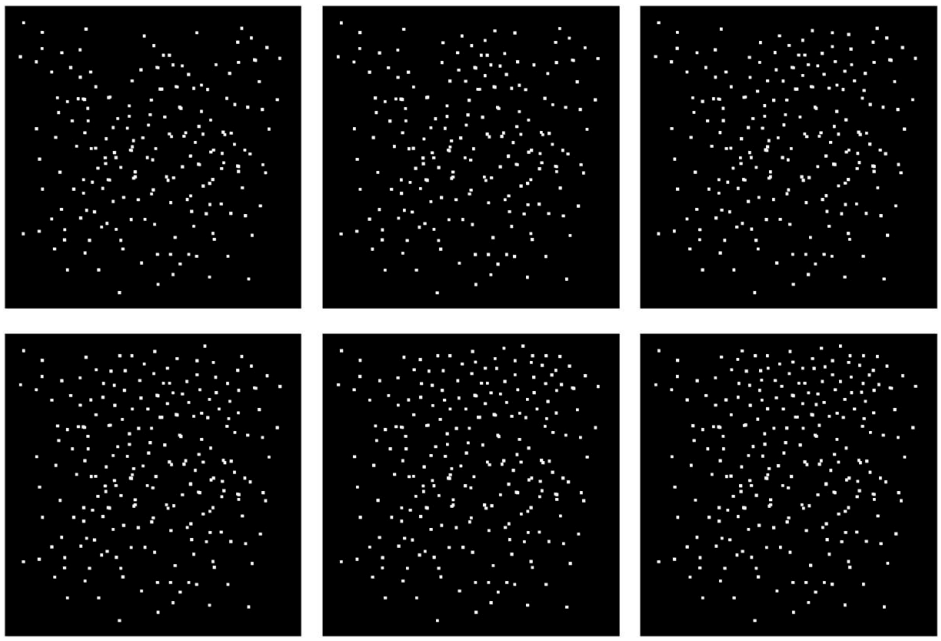

Figure 2: The randomly distributed white pixel content progressively increases between the first and last image of the series.

In a first time series of six images (Figure 2), the percentage of randomly distributed white pixel content increases regularly from +10% in the second image to +60% in the last image of the series, starting from an original reference image, which is the first of that series. The luminance intensity of white and black image contents was measured with a standard photosensitive lens driven by appropriate software (Cambridge Systems). The luminance of white pixel contents was constant at 60 cd/m^2 across images, the luminance of black pixel contents was constant at 2 cd/m^2 in all the images of the following series. Only the spatial extent of local contrast was varied here.

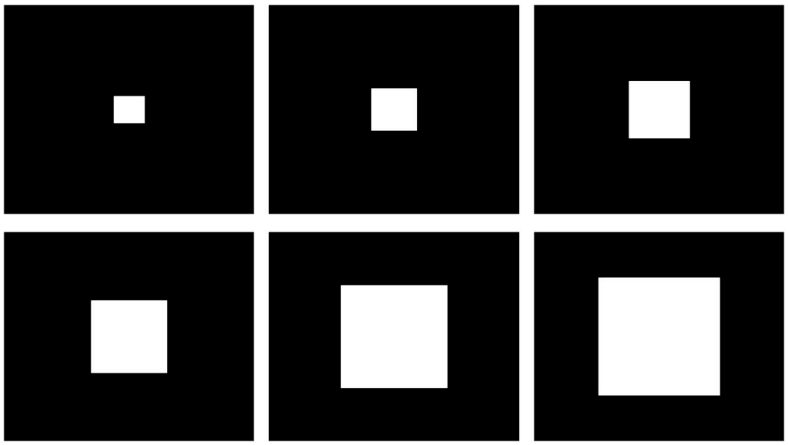

Figure 3: The percentage of the centrally placed white pixel content progressively increases between the first and last image in this series here.

In the fourth time series here, with six images (Figure 5), the percentage of centrally extending white pixel content in the shape of a square at the center of these images increases regularly from 1% in the first image to 32% in the last image of the series.

Preprints (www.preprints.org) | NOT PEER-REVIEWED | Posted: 20 March 2018 doi:10.20944/preprints201710.0166.v2

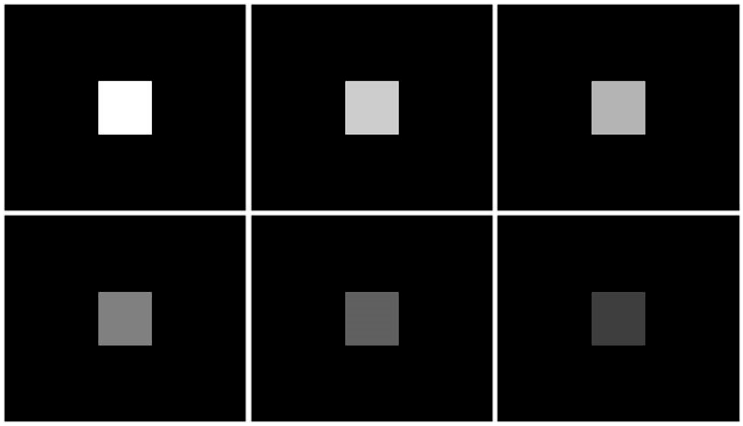

Figure 4: The test images from the sixth series for the proof-of-concept simulations testing for QE sensitivity to progressive increase/decrease in the intensity of contrast when spatial extent is kept constant across images of a series. The original series and a contrast-intensity-corrected version were submitted to SOM for comparison.

Identically sized images with gradually varying contrast intensity of a central contrast area with constant spatial extent across images were generated for this time series to finalize the proof-of-concept simulations (Figure 6). The original series with varying intensities and a contrast-intensity-corrected version using

$$I_{final} = (I - I_{min}/I_{max} - I_{min}) \times 255 \qquad (3)$$

were submitted to SOM for comparison.

A four-by-four SOM with sixteen artificial neurons was implemented, with an initial neighborhood radius of 1.2 and a learning rate of 0.2. SOM learning was performed on the last image of each time series. The neural network was set to learn in 10.000 iterations (*i*), producing Self-Organizing mapping output after learning in terms of final synaptic weights and their quantization error (QE). The results from these analyses, in terms of the quantization errors after learning obtained from SOM on images from each of the five different series, are represented graphically in the following section as a function of the image series SOM was run on. Linear regression analyses were performed to test the statistical significance of the QE variations as a function of the variations in the images.

2.2. Results

The quantization error from SOM on each image of each of the time series was plotted as a function of the increase (%) in spatial pixel content across images of a given series. These results are shown here below (Figures 5-7). As a given extent of spatially distributed contrast increases across images of a given time series, the QE from the SOM output also increases. The results from linear regression analysis show excellent goodness of the linear fits, as revealed by the linear regression coefficients $\boldsymbol{R^2}$, with statistically significant trends as revealed by the $\boldsymbol{t}$ values from the corresponding Student distributions. $\boldsymbol{R^2}$, $\boldsymbol{t}$, and the probability limits $\boldsymbol{p}$ of statistical significance are given in the legend of each Figure.

Preprints (www.preprints.org) | NOT PEER-REVIEWED | Posted: 20 March 2018 doi:10.20944/preprints201710.0166.v2

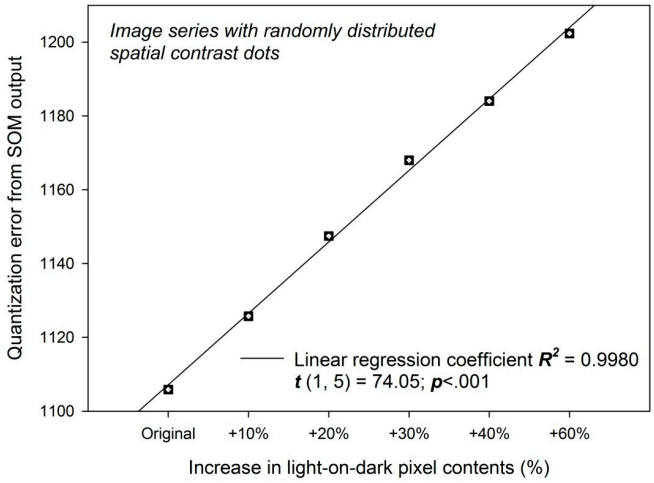

Figure 5: Variations in QE output plotted as a function of spatial extent of contrast in terms of number of randomly distributed white dots on the black image background. QE values are taken from the SOM on each of the six images of the first series here. When the intensity of contrast is constant across images, as is the case here, the QE is shown to increase linearly with the increase in spatial extent of contrast expressed in % of the total image area. The linear trend is statistically significant as shown here by the *t* value from the Student distribution of the raw data and the associated probability limits (*p*).

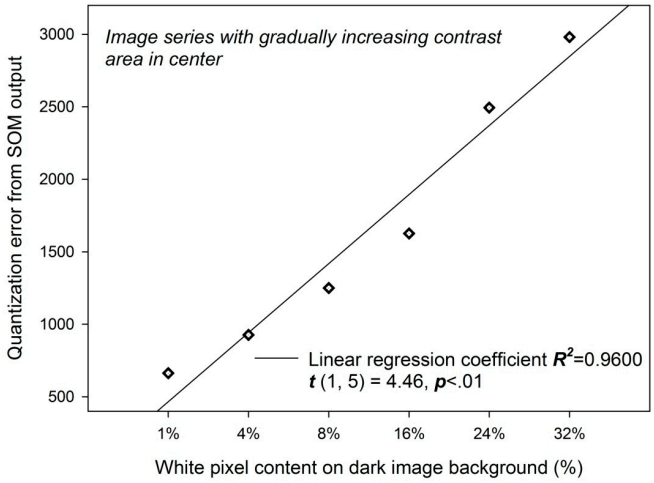

Figure 6: Variations in QE output plotted as a function of increasing contrast area at the center of the black image background. QE values are taken from the SOM on each of the six images from the second series here. Again, the QE is shown to increase linearly and significantly with the increase in spatial extent of contrast.

Preprints (www.preprints.org) | NOT PEER-REVIEWED | Posted: 20 March 2018 doi:10.20944/preprints201710.0166.v2

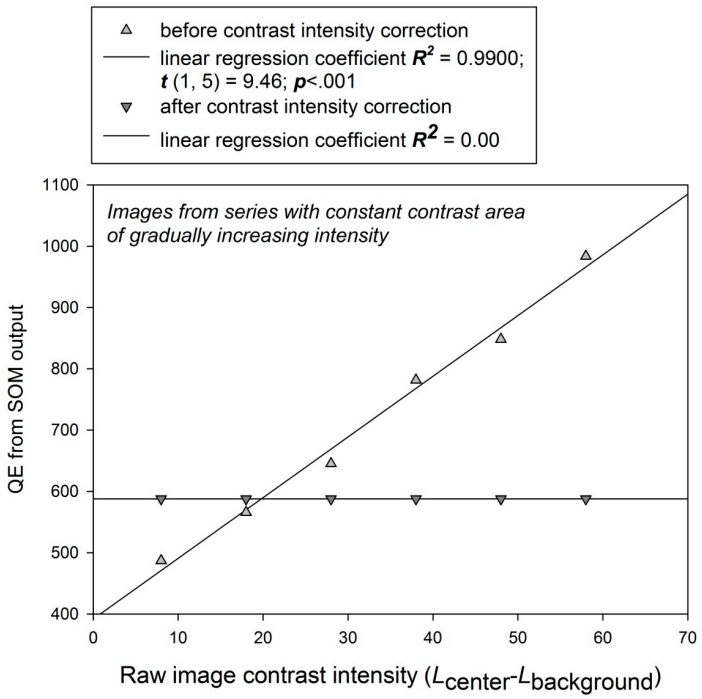

Figure 7: Significantly increasing QE output as a function of increasing contrast intensity of the area at the center of the black image background when the spatial extent of that areas is kept constant across images. QE values are taken from the SOM on each of the six images of the fifth and last series described in the Materials and methods section of Chapter 2. The QE is shown to increase linearly and significantly with the increase in contrast intensity across the images. After contrast intensity correction of the images from this series using the transform given here above in the Materials and methods section of Chapter 2, the QE from the SOM run on these transformed images is shown to remain constant.

The simulations shown here above provide substantial proof of concept beyond any reasonable doubt that the QE from the SOM output is a statistically reliable indicator of spatial changes in image regions under the condition that the intensity of contrast is constant across images of a given series. On the basis of these results, it will be made sure that all further analyses of image time series presented here are run on series of images with constant contrast intensities, if necessary preprocessed using the contrast intensity correction transform given above to ensure this condition holds for any given image series. This opens perspectives for the fast automatic pre-analysis of large bodies of images. In the medical fields these could be scans or MRI images taken over time from one and the same patient with a given critical condition the evolution of which is slow and progressive and hard to detect in the medical images, for example. The algorithm for SOM learning is easy to implement and the computational times for whole set of analyses are of a few seconds, bearing in mind that SOM performs a global analysis of the entire image. This opens new doors for complex problems such as the monitoring cancer progression/remission, which is often performed via manual segmentation of several images in an MRI sequence, which is prohibitively time consuming, or via automatic segmentation, a challenging and computationally expensive task that may result in high estimation errors [22]. The QE allows to almost instantly get some idea of the likelihood of change in terms of progression or remission, in real-time, directly from image statistics

 doi:10.20944/preprints201710.0166.v2

using the self-organizing machine learning technique. Moreover, the QE value of the output of these analyses detects even the smallest changes in potentially relevant local image contents that are impossible for humans to see, even when they are expert radiologists [18]. In the next section, we will compare the QE distributions from SOM run on time series of original imaging data from a patient before and after blunt force traumatic injury to test whether the QE consistently and reliably detects the change in the medical images across time. In a further step, artificial lesion-like content is added to medical images and SOM analyses are run on these modified images. This is similar to what was done in previous work [52] prior to further computational analyses using a metric of visual classification by an expert.

3. Change detection in time series of medical images

In medicine, the annotation of image data is subject to considerable differences between individuals, even when they are highly specialized experts such as radiologists [21]. The analysis of medical images assisted by computer techniques therefore represents a highly complex challenge. Radiologists have to assess the progression of patients' conditions on the basis of often hardly detectable, local changes in medical images. These are captured through various imaging techniques, such as magnetic resonance imaging (MRI), computerized tomography (CT), and positron emission tomography (PET), providing the radiologist with visual information about the state or progression of a given condition and helping to determine the course of treatment. Traditional methods for handling medical images involve direct visual inspection, which is by its nature subjective. Image science therefore has proposed methods for reducing subjectivity by introducing automated procedures. This involves various different image processing techniques aimed at identifying specific diagnostic regions, so-called regions of interest, and specific features representing tumors and lesions. For example, to avoid time-consuming voxel-by-voxel comparison for detecting changes between two images, the images can be aligned and displacement fields may be computed for recovering apparent motion by using a non-rigid registration algorithm [22]. This and similar techniques focus on the detection of regions of interest, with tumors or evolving lesions. A computer algorithm compares multiple series of images to produce a map of the changes, and expert knowledge is then applied to that map in a series of post-processing steps in order to generate a set of metrics describing the changes occurring in the images. During this process, domain-specific knowledge needs to be introduced, which attempts to reduce the impact of subjectivity by incorporating generic information an expert might use when annotating medical images manually. This, however, does not completely eliminate subjectivity.

Other approaches [23, 24] have proposed a computational framework to enable comparison of MRI volumes based on gray-scale normalization, to determine quantitative tumor growth between successive time intervals. Specific tumor growth indices were computed, such as volume, maximum radius, and spherical radius. This approach also requires the initial manual segmentation of the images, which is a time-consuming task. Semi-automatically segmenting successive images and then aligning them on the basis of hierarchical registration schemes has also been proposed for measuring growth or shrinkage in local image details [25]. All these methods rely on the accuracy of segmentation and require manual annotation for classifying local changes in pathology of up to a few voxels. Other methods [26, 27] which combine input from a medical expert with a computational technique are more specifically aimed at difficult-to-detect brain tumor changes. These methods, again, involve a subjectivity factor which is problematic given the well-known inter-individual differences between experts [21]. Our SOM approach to the problem of change detection of time series of medical images considers

Preprints (www.preprints.org) | NOT PEER-REVIEWED | Posted: 20 March 2018 doi:10.20944/preprints201710.0166.v2

the whole image as opposed to an image segment of a specific region of interest. Such an approach of direct analysis of the medical image as a whole has the advantage of not requiring manual benchmarking. The basic idea behind direct analysis is that there exists an intrinsic relationship between images with varying contents and their clinical significance, and that this relationship can be exploited directly without additional not necessarily reliable intermediate procedures of image processing. Compared to some of the traditional methods briefly reviewed here above, the method used here has a deeper meaning in the sense that it is close to the most natural approach to the problem. It directly targets the final outcome of change detection like a medical expert would, and thereby bridges the gap between machine learning and the classic medical image inspection approach of the human expert. A medical expert such as a radiologist explores imagers from a time-series as a whole and one by one to monitor the progression of a patient's conditions. Like the SOM, he/she derives diagnostic information from this "natural" procedure to reach a decision on the likely progression or remission of a condition such as a tumor or lesion, thereby evaluating the likely progress of a patient's state or response to therapy. This classic visual method of determining differences between one series of images to another can, however, fail to detect very small differences. This can be overcome by using fast SOM learning algorithms, generating quantization errors for rapid automatic change detection in medical image data.

Here, the power of QE to capture critical local changes is tested on time series of MRI images from a single patient before and after traumatic blunt force injury to the knee. In further simulations on MRI images to which *Poisson* noise or synthetic local lesion content were progressively added, it is shown that the QE consistently detects minimal changes in medical image data fast. It is suggested that the SOM algorithm generating the QE output data could be implemented to assist human experts such as radiologists in image-based decision making.

3.1. Materials and methods

A 16 by 16 SOM with an initial neighborhood radius of 5 and learning rate of 0.2 was set up for image learning. These initial values were obtained after testing SOM with different numbers of neurons to make sure that the cluster structures show sufficient resolution and statistical accuracy [28]. The learning process was started with vectors picked randomly from the image array as the initial values of the model vectors. Across the three SOM learning experiments, the parameters of the SOM were kept constant.

In the first experiment, SOM was run on two sets of 20 images from a patient with a traumatic knee injury courtesy of CHU de Hautepierre, Strasbourg, France. The same acquisition parameters were used to acquire the image sets which consisted of time series of 20 MRI images each. The 40 original MRI images from these two time series are shown in the Supplementary Materials section. SOM was applied to the two time series of original images, taken on two separate dates, before and after blunt force traumatic injury.

In the second experiment, artificial lesion content was added to these same images and SOM analysis was run on the modified images. In a previous study [52] original images were modified in a similar way by adding synthetically evolving pathological content of 1%, 5% and 22% volume growth prior to further analyses in terms of visual recognition experiments testing whether the artificial pathologies would be detected by medical expert. Here, we use SOM instead, which was not done in that previous study. On the first MRI time series, synthetic lesion content was added by adding higher contrast pixels locally to each original image to form a new set of images. Since the

Preprints (www.preprints.org) | NOT PEER-REVIEWED | Posted: 20 March 2018 doi:10.20944/preprints201710.0166.v2

aim was to reinforce changes within the images between time series, the new set of images retained all the characteristics of the first set, except for an additional lesion content, which was uniformly positioned in the 20 images of a series, Thereby, introducing synthetic lesion contents ensures that the differences between sets of images are not influenced by external factors like location of camera, lighting, the patient's position on the MRI machine and so forth. Furthermore, the spatial extent of the introduced lesion content is known. Here, it was a 44 by 26 pixels elliptic shape with 72 by 72 dpi gray-scale resolution.

To test another, maybe less arbitrary, way of adding synthetic lesion contents to original medical images, a Poisson frequency distribution was added to each image of the two MRI time series. Examples are shown here below (Figure 8). Poisson noise may be preferred to adding digital noise such as pixels for the generation of synthetic impurities because Poisson noise is mathematically *correlated* with the contrast intensity of each pixel in the image. The process produces a sample image from a Poisson distribution for each pixel of the original image. The same Poisson distribution parameters were applied to both time series. By its nature, the Poisson method populates the image with noise in proportion to existing pixels.

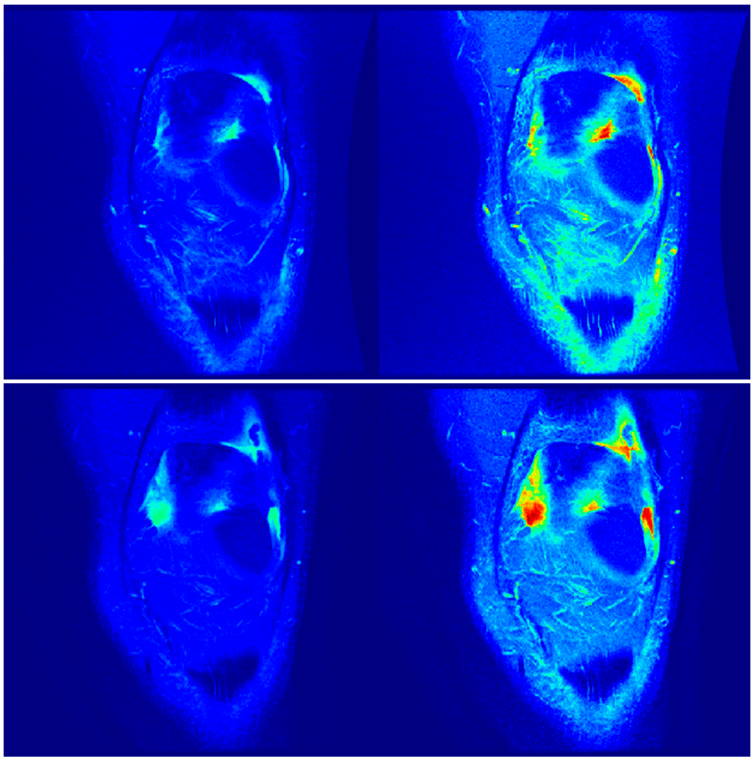

Figure 8: Samples of MRI images (courtesy Dr. P Choquet, CHU Strasbourg) taken on the first (top left) and second (bottom left) clinical visit, before and after traumatic injury. On the right, the same images after adding *Poisson* distributed noise, which represents a way of adding lesion contents synthetically and is less arbitrary compared with adding pixels locally.

3.2. Results

The *QE* values obtained from the SOM output for each set of the original image time series are shown here below.

Preprints (www.preprints.org) | NOT PEER-REVIEWED | Posted: 20 March 2018 doi:10.20944/preprints201710.0166.v2

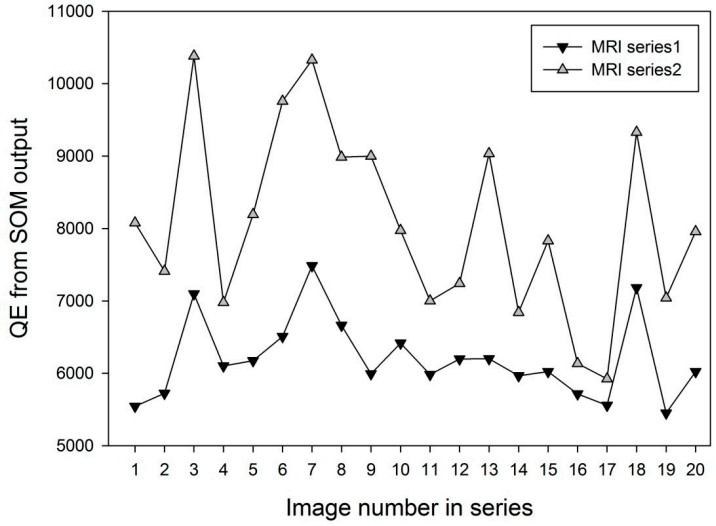

Figure 9: Results from SOM analyses on time series of the original MRI images, taken at two different moments in time, before (series 1) and after (series 2) blunt force trauma. It is shown that the *QE* increases significantly (***t*** (1, 38) = 3.336; ***p***<.01) between image series taken before and after the clinically significant event. The QE is a statistically reliable detection measure of the change between the images from the two series.

The QE distributions were submitted to one-way analysis of variance (ANOVA), which signaled that differences in QE from SOM run on the two image series is statistically significant (***t*** (1, 38) = 3.336; ***p***<.01). This significant difference in the QE distributions directly reflects the clinical significance of the image differences between the first and the second visit, in other words the effects of blunt force traumatic injury on the image series.

The results from SOM on the image series with added artificial lesion content similarly produced systematic increase in the *QE* between original image series and processed image series. These *QE* distributions (Figure 10) were also submitted to one-way analysis of variance (ANOVA). The differences between the QE distributions for the two series are also, as would be expected, statistically significant (***t*** (1, 38) = 5.61; ***p***< .01 and ***t*** (1, 38) = 2.18; ***p***<.05 respectively).

The results from SOM run on the original MRI image series with and without Poisson noise are also shown here below (Figure 11). Adding Poisson noise to the original MRI images produces differences in the *QE* distributions that are, again, statistically significant (***t*** (1, 38) = 20.76; ***p***< .001 f and ***t*** (1, 38) = 9.68; ***p***< .01 for series 1 and 2 and their modified versions, respectively). It is thus shown that adding Poisson noise to the original MRI images from the two series produces very similar results to those obtained from image series with added pixel contents to simulate artificial lesion growth.

Preprints (www.preprints.org) | NOT PEER-REVIEWED | Posted: 20 March 2018 doi:10.20944/preprints201710.0166.v2

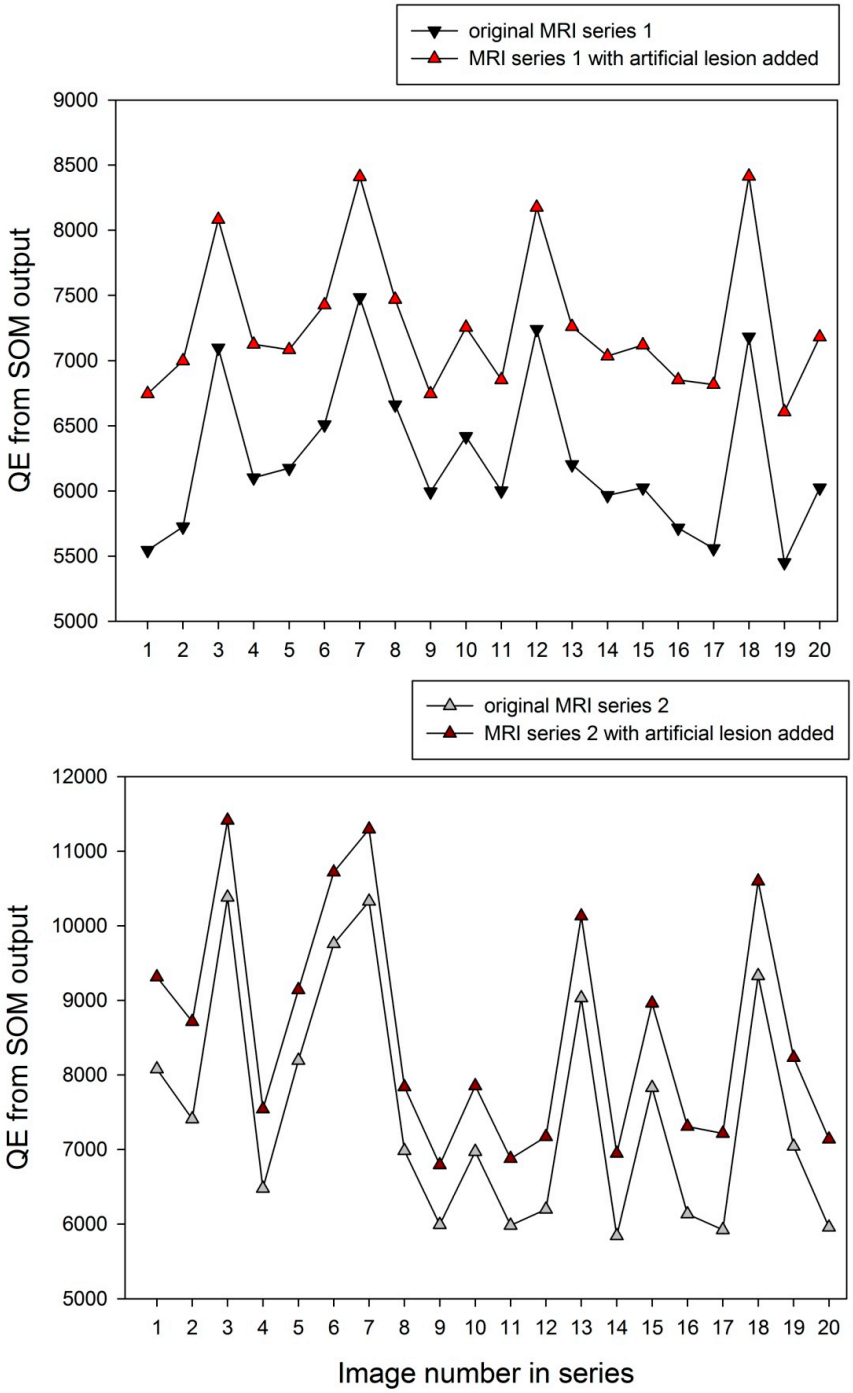

Figure 10: To the original images from the two series synthetic lesion content was added: a smaller one to the originals from series 1 and a larger one to the original images from series 2. The differences in the QE distributions are statistically significant for both.

Preprints (www.preprints.org) | NOT PEER-REVIEWED | Posted: 20 March 2018 doi:10.20944/preprints201710.0166.v2

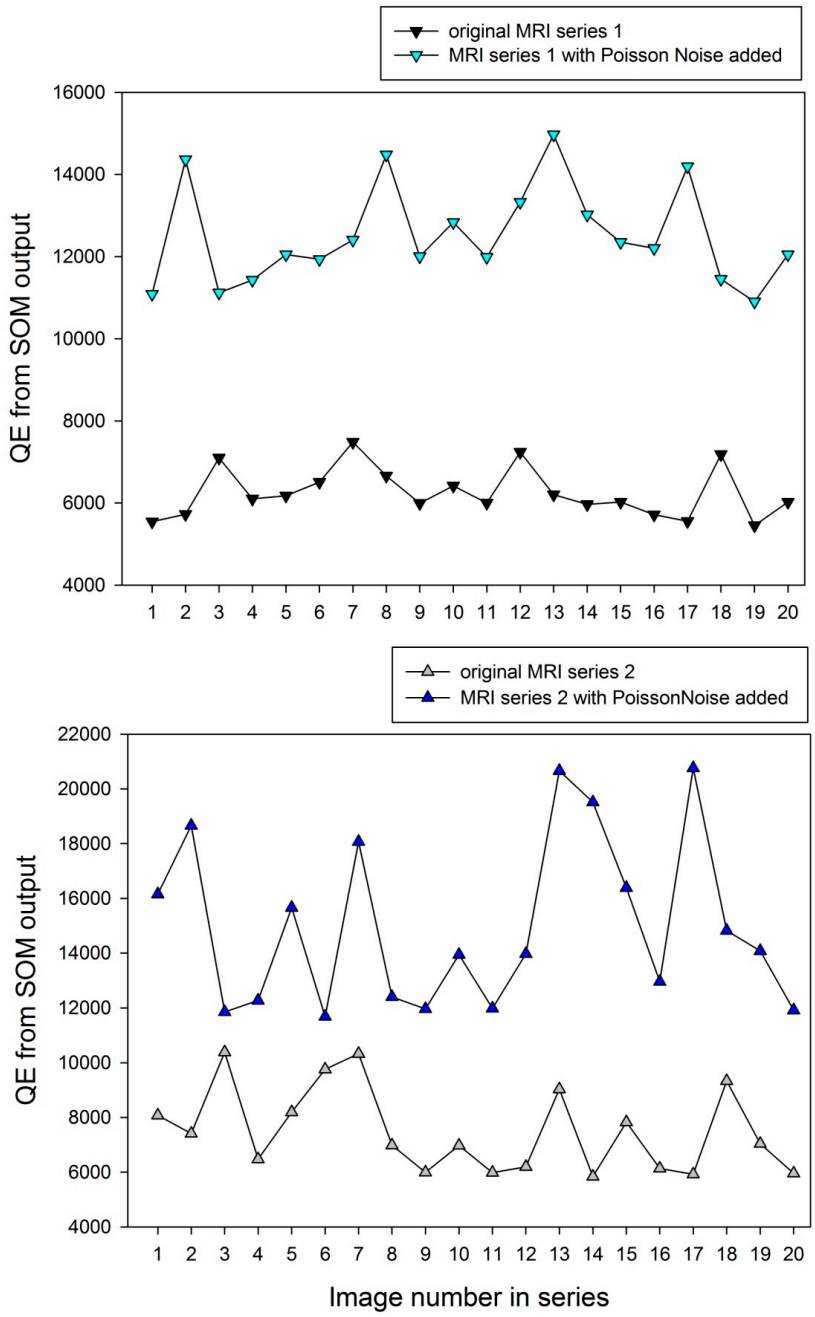

Figure 11: *QE* values from SOM of the set of original images taken from the patient on the first and second clinical visit (series 1 and 2), and on the same images with Poisson noise added.

3.3. Discussion

Biomedical signal and image processing focuses on different goals in the educational and research fields of biomedical engineering [57-98]. With growing physiological knowledge, a wider range of innovative research on clinical methods makes use of such processing in medical applications, and many advanced algorithms in the signal and image processing field rely on time frequency representation approaches, especially in the field of the neurosciences [93-97] and in functional imaging of the cardiovascular system [64-68, 72, 81].

 doi:10.20944/preprints201710.0166.v2

In this much advanced domain, some imaging modalities are now widely accessible and can deal with the progression of a disease to provide diagnostic information. This, however, involves multiple steps of computational analysis and processing and does not straightforwardly enable instant decision making. The future in this vast field of investigation will be comparing the performances of the most advanced algorithms and methods using a fusion of different techniques and functional imaging, with a high premium placed on ultrasound imaging [65-67, 69]. It is important here to point out that a deeper analysis of all these different approaches would be beyond the scope of this article, which is aimed at testing a simple method of fast and almost instant change detection that can be applied to ANY output image generated by ANY of the different biomedical imaging approaches. By this virtue, the simple method described here has the potential to aid human observer performance faced with any imaging data, and to help sharpen medical expertise and decision making [18, 99, 100, 101]. How QE output data may indicate critical change across image contents when compared with human detection using the same image material is discussed in detail in previous work from our group [18, 19] in the light of concepts from signal detection theory [17, 99].

The results from the series of simulations described in this chapter here suggest that the QE from SOM analysis seems well-tailored for fast change detection in large bodies of medical images from patients. It allows the automatic detection of subtle but significant changes in time series of images likely to reflect growing or receding lesions. In clinical practice, finding evidence for subtle growth through visual inspection of serial imaging can be very difficult. This is especially true for scans taken at relatively short intervals (less than a year). Visual inspection often misses the slow evolution because the change may be obscured by variations in body position, slice position, or intensity profile between scans, for example [52, 55-57]. In some cases, the change can be too small to be noticed. Surgeons and oncologists frequently compute the change in tumor volume by comparing the measurements from consecutive scans. When the change in tumor volume is too small and hence difficult to detect between two sequential scans, radiologists tend to compare the most recent scan with the earliest available image to find any visible evidence for an evolution of the tumor. The resulting analysis does, however, not reflect the current development of the tumor but rather a retrospective perspective of tumor evolution, as pointed out earlier [52, 55-75]. This study here addresses this problem, as fast SOM could be easily implemented to aid clinicians in deciding about treatment. The process of executing the code to determine the QE distribution for a series of twenty images takes about 40 seconds. This involves reading the DICOM images from a folder, running the SOM and determining the QE for each image, displaying the image on the screen and saving the QE value in a text file. In summary, whenever the QE from SOM on a patient's medical images taken at consecutive times rises, it is a potential indication that lesions or other pathological changes of the organ under study may be developing, while a decrease of the QE may indicate that a pathology is receding. To the best of our knowledge, our approach is the first to automatically detect potentially critical local changes in a patient by comparing images taken from subsequent clinical visits without relying on visual inspection or manual annotations. The SOM method detects these changes rapidly with a minimal computation time using consecutive images of an organ without having to rely on derived image qualities as is the case for image subtraction methods, for example [55, 56]. The SOM method also represents a clear advantage compared with monitoring a condition, for example cancer progression or remission, using manual segmentation techniques on each image from an MRI sequence, which is prohibitively time consuming.

In the human and environmental sciences, time-series of satellite images may

 doi:10.20944/preprints201710.0166.v2

reveal important data about changes in environmental conditions and natural or urban landscape structures that are of potential interest to citizens, historians, or policymakers. In the next section, we will show how the QE from SOM ran on extracts of satellite images for specific geographic regions of interest (gROI) can be used to detect relevant changes.

4. Change detection in time series of satellite images

Here, the Self Organized Map output in terms of the QE of the final synaptic weights after learning is applied for fast detection of critical changes in satellite images of specific gROI. These simulations are run on extracts of image time series of Las Vegas and its nearby surroundings in the Nevada Desert (USA), generated across the years 1984-2008, a period of major restructuration of the urban landscape of Las Vegas City and, at the same time, specific modifications of the natural landscape due to global climate change. As shown in the previous chapters, the QE from the SOM output is a reliable measure of variability in local image contents. In the present work, statistical trend analysis is used to show how the QE from SOM run on specific geographic regions of interest extracted from satellite images can be exploited for visualizing structural change across time at a glance, highlighting significantly correlated demographic data for a specific time period.

The detection and characterization of critical changes in public spaces of the natural or the built environment reflected by changes in image time series such as photographs or remotely sensed image data may be of considerable importance for risk mitigation policies and public awareness. This places a premium on fast automatic techniques for discriminating between changed and unchanged contents in large image time series, and computational methods of change detection in image data including remotely sensed data, exploiting different types of transforms and algorithms, have been developed to meet this challenge. Existing methods have been reviewed previously in excellent papers by [33] and [34]. Known computations include Otsu's algorithm [35], Kapur's algorithm [36], and various other procedures such as pixel-based change detection, image differencing, automated thresholding, image rationing, regression analysis on image data, the least-square method for change detection, change vector analysis, median filtering, background filtering, and fuzzy logic algorithms [37-47]. The scope of any of these methods is limited by the specific goal pursued. As pointed out previously, image change detection involves being able to reveal critical changes through analysis of discrete data sets drawn from image time series. One of the major applications concerns remotely sensed data obtained from Earth-orbiting satellites. These provide image time series through repetitive coverage at short intervals with consistent image quality [33].

Here, extracts from satellite images representing specific geographic regions of interest of Las Vegas County were used as input to SOM. After preprocessing to ensure equivalence in scale and contrast intensity of the extracted images within a time series, the image input is exploited directly without additional or intermediate procedures of analysis. To control for differences in intensity across images of a given time series, a transform is applied before running SOM on each extracted image of a time series. Then, the *QE* output distributions from SOM on adequately preprocessed extracts from satellite images of Las Vegas County generated across the years 1984-2008 are examined. The satellite image extracts correspond to three distinct gROI: Las Vegas City Center, Lake Mead and its close surroundings in the Nevada Desert, and the residential North of Las Vegas. The reference time period chosen for this study here (1984-2008) is of particular interest because of major structural changes in the urban landscape of Las Vegas City and the residential North during that period, and the gradual dwindling of nearby Lake Mead's

Preprints (www.preprints.org) | NOT PEER-REVIEWED | Posted: 20 March 2018 doi:10.20944/preprints201710.0166.v2

water levels due to the effects of global climate change. We use statistical trend analysis to prove that:

1) the QE distributions from the SOM on the different images corresponding to the gROI under study reliably reflect these critical changes across the years

2) the QE output is significantly correlated with the most relevant demographic data for the same reference time period.

4.1. Materials and methods

The images used for analysis of geographic regions of interest by SOM were extracted from time-lapse animations of Las Vegas City and Lake Mead, Nevada, from 1984-2008, as captured by NASA Landsat sensors.

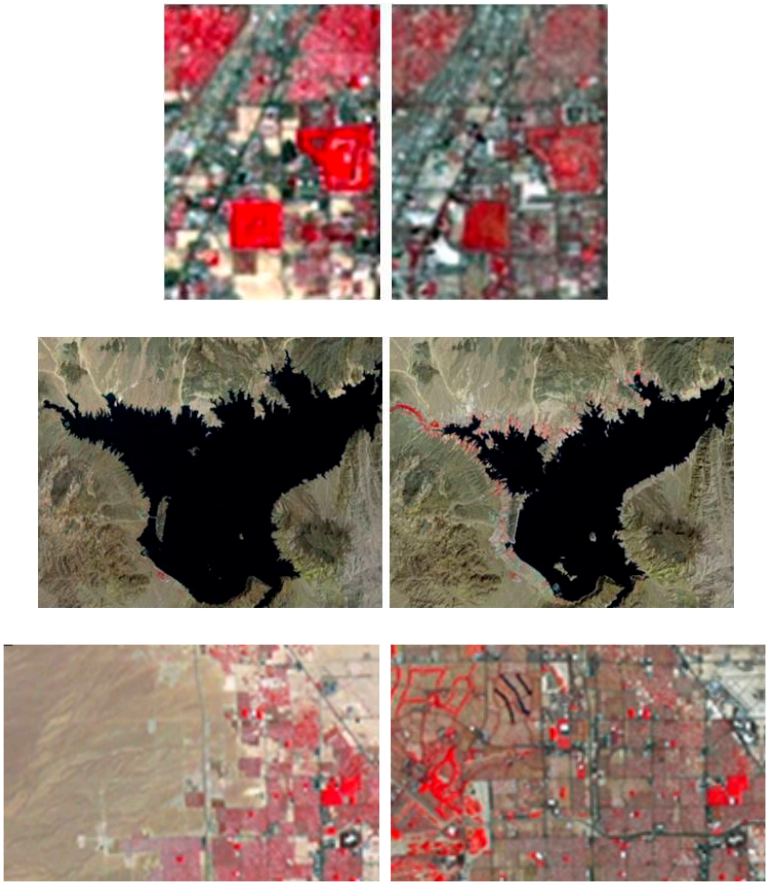

Figure 12: Examples of images extracted from the NASA Landsat database showing *three* gROI. Pre-processed images of *1)* Las Vegas City from the years 1984 and 2008 are shown at the top, pre-processed images of *2)* the region around Lake Mead from years 1984 and 2008 are shown in the middle, and preprocessed extracts from images of *3)* the residential North for 1984 and 2008 are shown at the bottom.

VLC, an open source media, was used to extract the images from the time-lapse animations provided. The images are false-color, showing healthy vegetation in red while

Preprints (www.preprints.org) | NOT PEER-REVIEWED | Posted: 20 March 2018 doi:10.20944/preprints201710.0166.v2

water is in black. Samples of the 25 images extracted for each of the three geographic ROI, Las Vegas City, Lake Mead, and the residential North are shown here (Figure 12).

Before running SOM on the time series for each geographic ROI, the images were pre-processed to ensure that images from a same subset are aligned. This was achieved by applying the method of co-registration using *StackReg*, which is a plug-in for *ImageJ*, an open source image processing program designed for scientific multidimensional images. From each image series for the two geographic ROI, the last image was used to anchor the registration. Control for variations in contrast intensity between images of a series was performed after registration. This was achieved by increasing the image contrast and by removing any local variations at different times of image acquisition. For each extracted image, contrast normalization was obtained using

$$I_{final} = (I - I_{min}/I_{max} - I_{min}) \times 255$$

The registered and normalized image taken in 2011 from each ROI was used to train a 4 by 4 SOM with a neighborhood distance of 1.2 and a learning rate of 0.2 for 10,000 iterations. Since the original images used color to emphasize different areas on the maps, pixel-based RGB values are used as input features to the SOM. This ensures a pixel-by-pixel capture of detail and avoids errors due to inaccurate feature calculation which often occur with complex images. With the trained SOM, QE values were determined for each of the 25 images of each geographic region of interest from the years 1984-2008. The QE values were fed into linear regression analysis. Correlation analysis using Pearson's method were performed to establish the statistical significance of correlations between variations in QE and other demographic data for the same reference time period.

4.2. Results

QE results from SOM run on the time series of 25 image extracts for each of the three gROI (Las Vegas City Center, Lake Mead, and the residential North) are shown and discussed here in the light of their statistical significance from linear trend analysis. Pearson's correlation method is used to link the QE to a set of highly relevant demographic data from the same reference time period. Image extraction and preprocessing applied before SOM analysis, and the principles of SOM run on the different image series have been explained in the Materials and methods section here above.

Region of interest: Las Vegas City

This section deals with the results from SOM run after pre-processing (see Materials and Methods) on satellite image extracts of the geographic ROI Las Vegas City. The corresponding image ROI covers an area of 72 by 98 pixels. During the reference time period of this study, significant changes in building density across the whole of Las Vegas City has marked these years of major restructuration (1984-2008). Photographic snapshots taken of parts of the "Strip", the central artery of Las Vegas, where most attractions are located, illustrate some of these changes (Figure 13).

Preprints (www.preprints.org) | NOT PEER-REVIEWED | Posted: 20 March 2018 doi:10.20944/preprints201710.0166.v2

Figure 13: Photographic snapshots of parts of "The Strip" across the years 1982-2010. These photos, taken in 1984, 1995, 2005 and 2008 respectively, give some idea of the structural changes that took place in Las Vegas City during the reference time period of this study here, for which the satellite images generated by NASA were retrieved.

Results in terms of QE output of the SOMs for the 25 image extracts corresponding to the ROI Las Vegas City are shown here below (Figure 14) as a function of the year in which an image was taken. The variations in the QE shown reflect varying spatial contrast distribution in the images across time. These are indicative of the major structural changes in the urban landscape during the reference time period. Trend analysis (linear regression analysis) on these data reveals a trend towards increase in QE as a function of time expressed in terms of the progression in years of the reference period 1984-2008, with a linear regression coefficient R^2 = .48, and a t (1, 24) = 2.13, p<.05 indicating that the trend towards increase in QE with time is statistically significant. Contrast intensity across images of a time series for a given ROI being controlled for by preprocessing (see Materials and methods), the significant increase in QE from SOM output reliably signals a significant increase in spatial extent of contrast regions in the images with time. Trend analysis on related demographic data for Las Vegas City show that both the number of visitors in millions and the estimated total population in thousands have increased significantly over the reference time period. These data are shown here below (Figures 15 and 16).

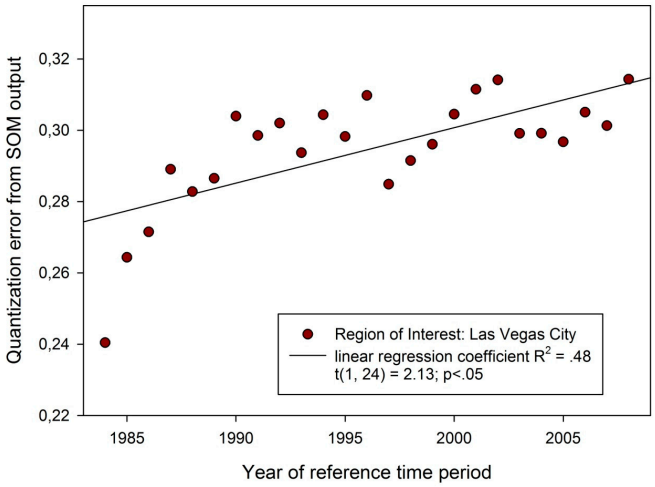

Figure 14: Variations in QE output plotted as a function of time. QE values are taken from the SOM on each of the 24 images corresponding to the geographic ROI 'Las Vegas City'.

Preprints (www.preprints.org) | NOT PEER-REVIEWED | Posted: 20 March 2018 doi:10.20944/preprints201710.0166.v2

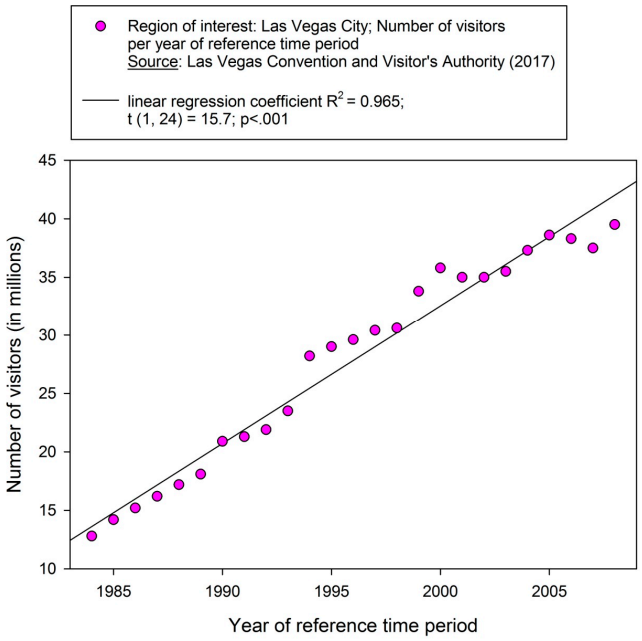

Figure 15: Number of visitors of Las Vegas City as a function of time. The linear trend yields a regression coefficient $\boldsymbol{R^2}$ = .965 and is statistically significant with $\boldsymbol{t}$ (1, 24) = 15.7, $\boldsymbol{p}$<.001.

To assess the statistical correlation between the QE and other relevant demographic variables from the reference time period here, we computed Pearson's correlation coefficient on the distributions for QE *vs* number of visitors and QE *vs* estimated population total. Pearson's correlation coefficient *R* gives an estimate of the statistical relationship, or association, between two independent continuous phenomena, or variables based on the mathematical concept of covariance.

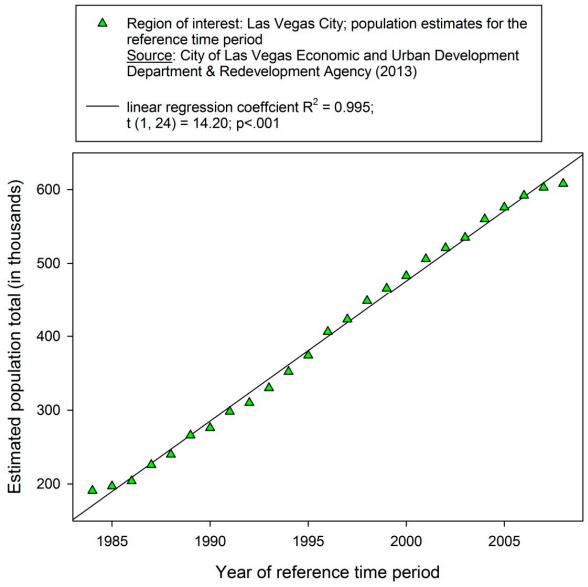

Figure 16: Estimated population total for Las Vegas as a function of time. The linear trend yields a regression coefficient $\boldsymbol{R^2}$ = .995 and is statistically significant with $\boldsymbol{t}$ (1, 24) = 14.2, p<.001.

Preprints (www.preprints.org) | NOT PEER-REVIEWED | Posted: 20 March 2018 doi:10.20944/preprints201710.0166.v2

R is associated with a probability *p* and carries information about the magnitude of the association, or correlation, as well as the direction of the relationship. Pearson's correlation statistic computed on the paired distributions signals statistically significant correlations between the QE and the number of visitors and between the QE and the population totals for the time period 1984-2008 on the gROI Las Vegas City.

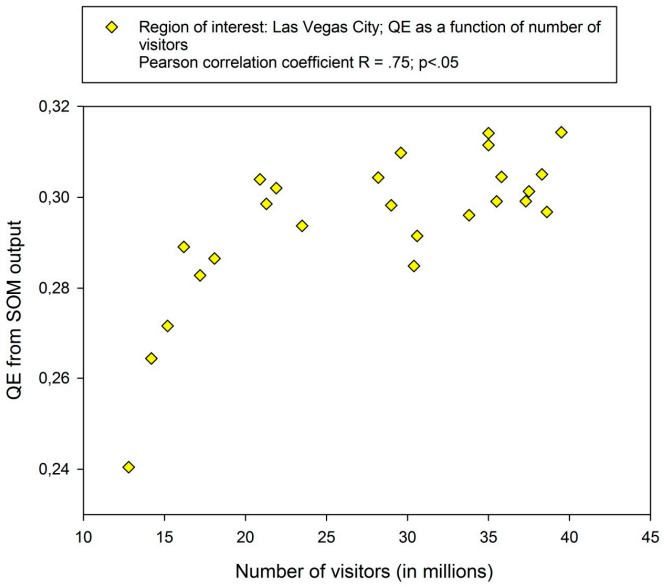

Figure 17: Variations in QE output plotted as a function of the number of visitors of Las Vegas City during the reference time period. Pearson's correlation statistic computed on paired distributions, plotted here in ascending order, gives a statistically significant correlation with $R = .75$, $p<.05$.

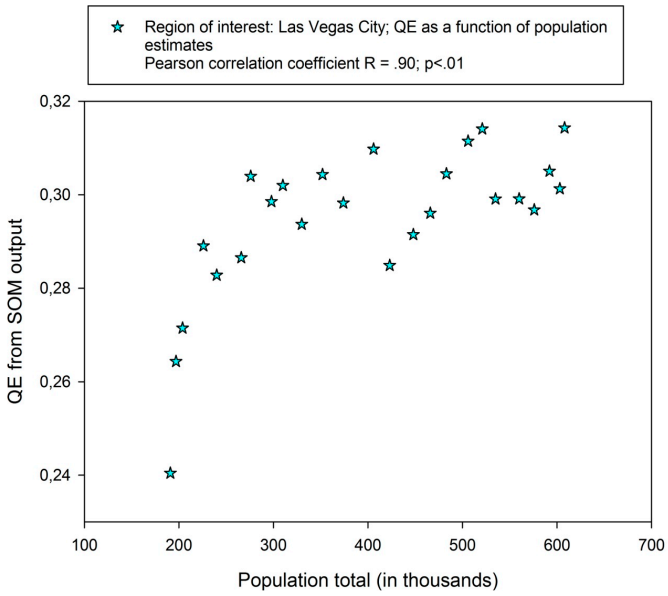

Figure 18: Variations in QE output plotted as a function of the number of estimated population totals for Las Vegas City during the reference time period. Pearson's

Preprints (www.preprints.org) | NOT PEER-REVIEWED | Posted: 20 March 2018 doi:10.20944/preprints201710.0166.v2

correlation statistic computed on the paired distributions, plotted here in ascending order, gives a statistically significant correlation with $R = .90$, $p<.01$.

Region of interest: Lake Mead Reservoir

This section deals with the results from SOM run after pre-processing (see Materials and Methods) on satellite image extracts of the geographic ROI Lake Mead. The corresponding image ROI covers an area of 430 by 366 pixels. Lake Mead is an artificial lake in the Nevada Desert collecting water from the Colorado River. Enclosed by Hoover Dam, the lake constitutes a reservoir serving water to the states of Arizona, California, and Nevada. Providing for nearly 20 million people and large areas of farmland, it is geographically situated 24 miles away from the Las Vegas Strip, southeast of Las Vegas City, Nevada, in the states of Nevada and Arizona. Lake Mead is the largest reservoir in the United States in terms of water capacity. During the reference time period of this study, Lake Mead water levels have progressively dwindled away as a consequence of global climate change. This phenomenon is captured by the QE from SOM run on the satellite image extracts, as shown here below (Figure 19).

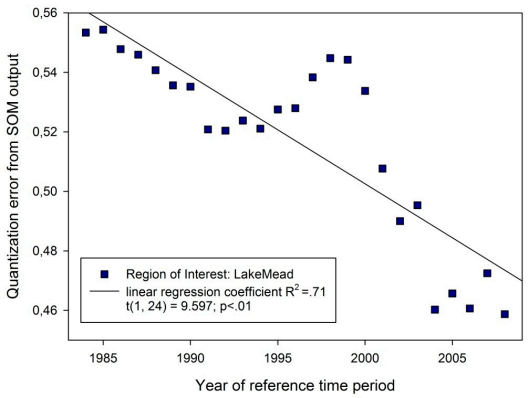

Figure 19: Variations in QE output plotted as a function of time. From SOM on image extracts for the gROI Lake Mead.

Trend analysis (linear regression analysis) on these data reveals a trend towards decrease in QE as a function of time expressed in terms of the progression in years of the reference period 1984-2008, with a linear regression coefficient $R^2 = .71$, and a t (1, 24) = 9.597, p<.01 indicating that the trend towards decrease in QE with time is statistically significant.

Contrast intensity across images of a time series for a given ROI being controlled for by preprocessing (see Materials and methods), the significant decrease in QE from SOM output reliably signals a significant decrease in spatial extent of contrast regions in the images with time. This image phenomenon is directly related to the shrinking away of Lake Mead, as can be seen in the image examples for 1984 and 2009 (see Materials and methods). Water level statistics for the reference time period are shown here below (Figure 20).

Pearson's correlation statistic computed on the paired distributions for *QE* and *water levels* signals a statistically significant correlation, shown here below (Figure 21), for the time period 1984-2008 on the gROI Lake Mead.

Preprints (www.preprints.org) | NOT PEER-REVIEWED | Posted: 20 March 2018 doi:10.20944/preprints201710.0166.v2

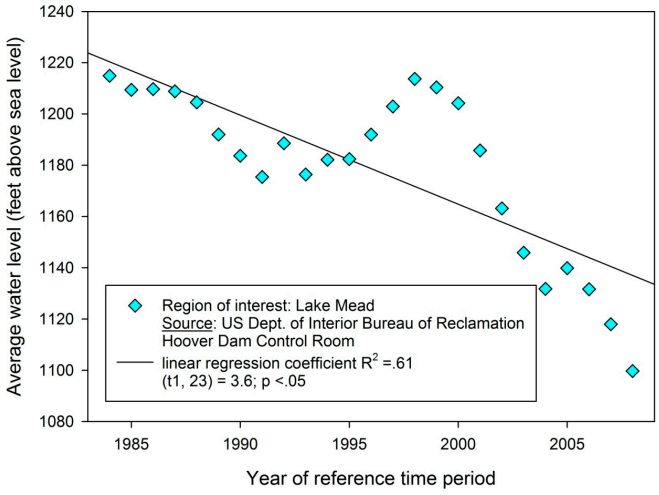

Figure 20: Water levels of Lake Mead as a function of time. The linear trend towards decrease yields a regression coefficient $\boldsymbol{R^2}$ = .36 and is statistically significant with $\boldsymbol{t}$ (1, 23) = 3.6, p<.05.

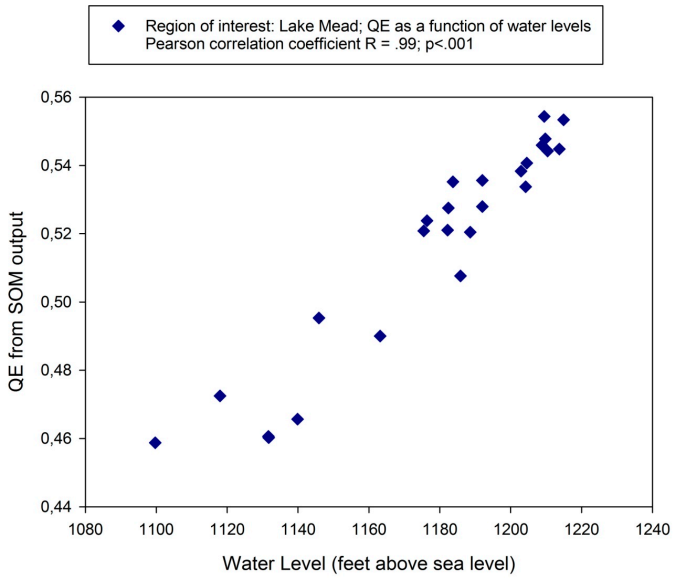

Figure 21: Variations in QE output plotted as a function of the water levels of Lake Mead during the reference time period. Pearson's correlation statistic computed on the paired distributions, plotted here in ascending order, gives a statistically significant correlation with R = .99, p<.001.

Region of interest: the residential North

The geographic region of interest is a section situated to the North of Las Vegas City, USA. The selected area encloses Sun City and North Las Vegas Airport to the left and right respectively. At the bottom of the image area (see Materials and methods) are the

Preprints (www.preprints.org) | NOT PEER-REVIEWED | Posted: 20 March 2018 doi:10.20944/preprints201710.0166.v2

Suncoast Hotel and Casino on the left and the Spring Preserve on right, all part of the image extracted from the satellite animation. During the years 1984-2008, a critical time period of real estate developments in this region, this part of Las Vegas was progressively transformed from desert to a densely built-up residential suburb. The false coloring in red in the images of this gROI shown in Materials and methods here above indicates healthy natural vegetation and other man-made green spaces, mostly golf courses, playgrounds, and parks. According to NASA, the image quality had improved considerably by then (1984, the first year of the reference time period here) as new instrument design improved the ability to resolve even smaller parcels of land. The significant changes in building density that have occurred in this geographic region of interest, turning the land from desert into a major densely built-up residential suburb of Las Vegas City, are well captured by the QE trend from the SOM output distribution after learning on the image series. The QE distribution for this gROI is shown here as a function of the year of the reference time period (Figure 22). Linear regression analysis on the *QE* data returned a regression coefficient $\boldsymbol{R^2}$ = .7999. The linear relationship between the artificial neural network (SOM) output in terms of *QE* and time is statistically significant with $\boldsymbol{t}$ (1, 24) = 33.45; $\boldsymbol{p}$<.001. This indicates that the artificial system reliably detects the critical structural changes in the images of Las Vegas North across time. The trend towards increased land cover in the North of Las Vegas is further illustrated by demographic data for that geographic ROI from the same time period, as shown here (Figure 23).

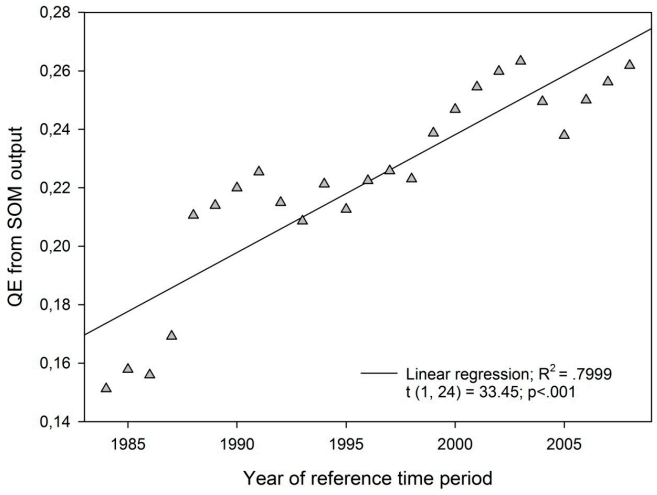

Figure 22: *QE* trend as a function of the year of the reference time period from which the input images were taken for the gROI residential North.

Regression analysis on these data returns a regression coefficient $\boldsymbol{R^2}$ = .92. The linear relationship between population estimates and time is statistically significant with $\boldsymbol{t}$ (1, 24) = 9.23, $\boldsymbol{p}$<.001. In a next step, we plotted the QE output of the artificial neural network as a function of these population estimates in ascending order. These results are shown here further (Figure 24).

Preprints (www.preprints.org) | NOT PEER-REVIEWED | Posted: 20 March 2018 doi:10.20944/preprints201710.0166.v2

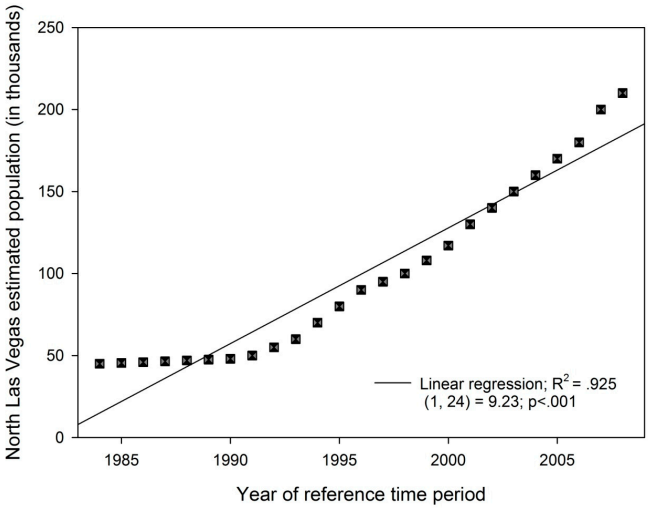

Figure 23: Population totals (estimates in thousands) as a function of the same reference time period.

The link between the increase in QE from the image analyses and the population estimates for the same geographic ROI Las Vegas North for the reference time period of this study is described by a positive Pearson correlation with $R = .51$.The QE output of the artificial neural network analysis of the image time series of Las Vegas North across the years 1984-2008 reliably reflects the progressive land cover changes in this geographic region of interest.

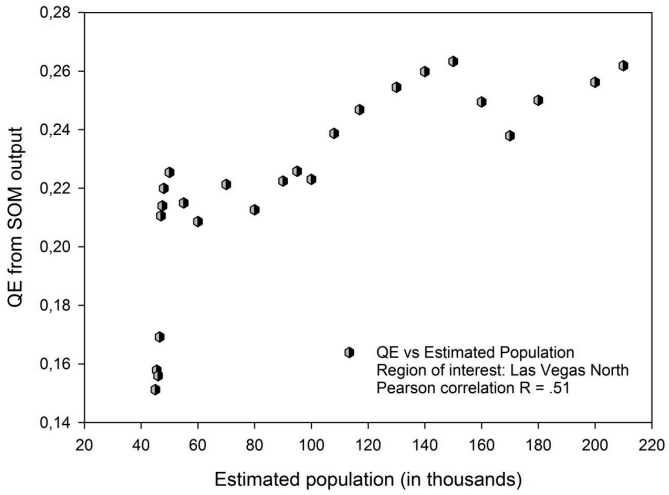

Figure 24: QE output from the image analyses as a function of the population estimates for the same geographic ROI Las Vegas North. The two variables are positively correlated as testified by Pearson's R

Preprints (www.preprints.org) | NOT PEER-REVIEWED | Posted: 20 March 2018 doi:10.20944/preprints201710.0166.v2

4.3. Discussion

The advantage of satellite data in Earth observation for environmental monitoring is considerable. The technological advances in spatial synchronization and temporal repeat observation of large areas over the years 1980-2018 [102-112] have significantly improved both the quantity and quality of landscape observation by satellite image data, which are becoming increasingly important in environmental monitoring. Because of the broad scale spatial coverage of satellite images, recording the data from the curved surface of the Earth in two-dimensional representations results in geometric distortions. With repeated coverage, radiometric consistency were previously hard to maintain between separate images due to different atmospheric conditions, variations in the solar illumination angles, and sensor calibration trends. Therefore, among the various aspects of progress in image data acquisition for land cover change detection and detection of other changes in natural landscapes (erosion, aridity, flooding etc.), there have been outstanding achievements over the years in the following

1) multi-temporal image generation
2) radiometric calibration

which had as a result that there is no longer much need for geometric correction of the satellite images. Previously, a standard geographic coordinate system was typically selected for images of interest to identify geometric ground control points on the satellite image and on the corresponding geographic coordinate system to derive a geometric relation between the two [102-113]. Nowadays, the satellite images are of a constant quality across time series and reflect geographic locations and relative distances between them much more reliably. Also, the imagery is not any more so much affected by climatic conditions.

In recent studies [114], up-to-date change detection methods applied to satellite images have been generally categorized as either supervised or unsupervised, according to the nature of data processing. The former is based on a supervised classification method, which requires the availability of a ground truth in order to derive a suitable training set for the learning process of classifiers. The latter approach, which is adopted here in this fast SOM approach, performs change detection by making a direct comparison of multi-temporal images from a series considered without incorporating any additional information. Others [114] have previously proposed a technique for unsupervised change detection in multi-temporal satellite images using principal component analysis (PCA) and k-means clustering. Therein, the difference between two image is partitioned into h times h non-overlapping blocks. Ortho-normal eigenvectors are extracted through PCA from h times h non-overlapping blocks and set to create an eigenvector space. Each pixel in the difference image is represented by an S-dimensional feature vector, which is the projection of h times h the difference image data onto the generated eigenvector space. Change detection is then achieved by partitioning the feature vector space into two clusters using k-means clustering with $k = 2$, and then assigning each pixel to one of the two clusters using the minimum Euclidean distance between pixels' feature vectors and mean feature vectors of clusters. Although this statistical method has proven effective for change detection at the pixel level, which makes it possibly as sensitive to small changes as is the unsupervised method proposed and tested here in this thesis, it involves pixel-by-pixel computation of local differences between no more than two images by algorithms that are much more time consuming than these of SOM.

In the SOM approach used here, a whole series of 20 or more images are

Preprints (www.preprints.org) | NOT PEER-REVIEWED | Posted: 20 March 2018 doi:10.20944/preprints201710.0166.v2

compared at the pixel level, generating QE output sensitive to change at the pixel level for entire dataset in a few minutes and thereby allowing to decide instantly (change/no change) about presence or absence of smallest localized changes across images of the whole time series. There is, to our knowledge, no other method capable of providing such an instant result at this level of analysis. A global localization of changed area is achieved here by selecting specific gROI where change is suspected. Finer analyses relative to exact pixel-by-pixel locations of change in remotely sensed data using SOM for feature mapping, which is the more classic approach [115, 116, 117, 118] can be run subsequently for a specific time if necessary. On the example of the gROI of Lake Mead selected here in this study, a decision maker might be alerted by the QE evolution in the data shown, and then decide he/she needs finer analyses for a specific year and region at the Lake to implement appropriate policies for risk mitigation at that location. Then, SOM approaches as described in [115, 116, 117, 118] would be adequate methods of choice.

The QE belongs to a type of quality measures that have been used to benchmark different SOMs trained on the same dataset [119], convergence criteria [120], or to assess the fault tolerance of SOM [121]. In our work, we have used QE to realize a generalized measure of variation across data in a series of datasets using SOM learning with exactly the same parameters. In other words, we use the same SOM, same map size, feature size, learning rate and neighbourhood radius to analyze series of image datasets with clinical significance, random-dot images, or remotely sensed image data as shown here. The QE is derived after subjecting an image to the self-organizing map algorithm analysis and by calculating the squared distance (usually, the standard Euclidean distance) between an input data x and its corresponding centroid, the so-called “best matching unit". Since this is easy to implement, fast, and reliable for what it is supposed to provide, an instant criterion for decision about change/no change in a whole series of images, it represents indeed a promising and non-expensive technique for the automatic tracking and harvesting of landscape-change information from large bodies of image data on the basis of, in principle, ready-to-use simulations. Such information relative to critical changes in environmental conditions and natural or urban landscape structures can, as shown here, be instantly correlated with other relevant demographic data which are of potential interest to citizens, historians, or policymakers.

Conclusions

Here, we have given a large body of proof of the relative power of the QE from SOM output by showing that the metric is sensitive to spatial extents of local image contrasts at constant intensity. Applied here to medical images and adequately preprocessed extracts from satellite images, the QE output from SOM reliably reflects spatial variability in image ROI corresponding to a specific ROI. The QE provides a statistically significant indicator of potentially important change in image contents across time which may reflect a critical evolution of man-induced and natural phenomena in these geographic regions of interest. Once again, it has to be pointed out that the major advantage of the method is the fast computation time and the fact that it can deal with a whole series of 20 or more images at a time. After some minimal preprocessing to control for equivalence in spatial scale and contrast intensity of images of a given image series, it takes hardly more than a minute to run SOM on a time series of 25 images, for example.

 doi:10.20944/preprints201710.0166.v2

Bibliography

[1] T. Kohonen, “Automatic formation of topological maps of patterns in a self-organizing system,” in *2nd Scand. Conf. on Image Analysis*, Espoo, Finland, 1981, pp. 214–220.

[2] T. Kohonen, *MATLAB Implementations and Applications of the Self-Organizing Map*. 2014 [Online]. Available: http://docs.unigrafia.fi/publications/kohonen_teuvo/

[3] Hubel , D.H. & Wiesel, T.N. (1959). Receptive fields of single neurons in the cat’s striate cortex. *The Journal of Physiology, 148*, 574-591.

[4] Hubel, D.H. (1963). Integrative processes in central visual pathways of the cat. *Journal of the Optical Society of America, 53,* 58-66.

[5] Hubel, D. H. & Wiesel, T. N. (1965). Receptive fields and functional architecture in two nonstriate visual areas (18 and 19) of the cat. *Journal of Neurophysiology, 28,* 229-289.

[6] Hubel, D. H. & Wiesel, T. N. (1968).Receptive fields and functional architecture of monkey striate cortex. *Journal of Physiology, 195*, 215-243.

[7] Dresp, B. (1998). The effect of practice on the visual detection of near-threshold lines. *Spatial Vision*, 11, 1-13.

[8] Wehrhahn C., Dresp B. (1998). Detection facilitation by collinear stimuli in humans: Dependence on strength and sign of contrast. *Vision Research*, 38, 423-428.

[9] Dresp, B. (2000). Do positional thresholds define a critical boundary in long-range detection facilitation with co-linear lines? *Spatial Vision*, 13, 343-357.

[10] Fischer, S., & Dresp, B. (2000). A neural network for long-range contour diffusion by visual cortex. *Lecture Notes in Computer Science*, 1811, 336-342.

[11] Dresp, B., & Fischer, S. (2001). Asymmetrical contrast effects induced by luminance and colour configurations. *Perception & Psychophysics*, 63, 1262-1270.

[12] Tzvetanov, T., & Dresp, B. (2002). Short- and long-range effects in line contrast detection. *Vision Research*, 42, 2493-249.

[13] Spillmann, L, Dresp-Langley, B, & Tseng, CH (2015) Beyond the classic receptive ield: The effect of contextual stimuli. *Journal of Vision*, 15, 7.

[14] Dresp, B., & Grossberg, S. (1997). Contour integration across polarities and spatial gaps: From local contrast filtering to global grouping. *Vision Research*, 37, 913-924.

[15] Carandini, M., Demb, J.B., Mante, V., Tolhurst, D.J., Dan, Y., Olshausen, B.A., Gallant, J.L., Rust, N.C. (2005). Do we know what the early visual system does? *Journal of Neuroscience, 25,* 10577-10597.

[16] Kapadia, M.K., Westheimer, G., & Gilbert, C.D. (2000). Spatial contribution of contextual interactions in primary visual cortex and in visual perception. *Journal of Neurophysiology, 84,* 2048-2062.

[17] J. A. S. David M. Green, *Signal detection theory and psychophysics*. New York: John Wiley & Sons, Inc., 1966. . New York: John Wiley & Sons, Inc., 1966

[18] J. M. Wandeto, H. Nyongesa, Y. Remond, and B. Dresp-Langley (2017) Detection of smallest changes in medical and random-dot images comparing self-organizing map performance to human detection. *Informatics in Medecine Unlocked*, 7, 39-45.

[19] J. M. Wandeto, H. Nyongesa, Y. Remond, and B. Dresp-Langley (2017) Detection of smallest changes in medical and random-dot images comparing self-organizing map performance and expert performance. *European Conference on Visual Perception (ECVP)*, Berlin.

[20] Dresp, B., Durand, S., & Grossberg, S. (2002). Depth perception from pairs of stimuli with overlapping cues in 2-D displays. *Spatial Vision*, 15, 255-276.

[21] S. J. van Riel, C.I. Sánchez, A. A. Bankier, D. P. Naidich, J. Verschakelen, E.T. Scholten et al. (2015). Observer variability for classification of pulmonary nodules on low-dose CT images and its effect on nodule management. *Radiology* 277, 863–871. doi:10.1148/radiol.2015142700

[22] D. Rey, G. Subsol, H. Delingette, and N. Ayache, "Automatic detection and segmentation of evolving processes in 3D medical images: Application to multiple sclerosis," *Medical image analysis*, vol. 6, no. 2, pp. 163–179, 2002 [Online]. http://www.sciencedirect.com/science/article/pii/S1361841502000567.

[23] J. Patriarche and B. Erickson, "Part 2. Automated Change Detection and Characterization Applied to Serial MR of Brain Tumors may Detect Progression Earlier than Human Experts," *Journal of Digital Imaging*, vol. 20, no. 4, pp. 321–328, Dec. 2007 [Online]. Available: http://link.springer.com/10.1007/s10278-006-1039-0.

[24] E. D. Angelini, J. Atif, J. Delon, E. Mandonnet, H. Duffau, and L. Capelle, "Detection of glioma evolution on longitudinal MRI studies," in *2007 4th IEEE International Symposium on Biomedical Imaging: From Nano to Macro*, 2007, pp. 49–52 [Online]. http://ieeexplore.ieee.org/xpls/abs_all.jsp?arnumber=4193219.

[25] E. D. Angelini, J. Delon, L. Capelle, and E. Mandonnet, "Contrast mapping and statistical testing for low-grade glioma growth quantification on brain mri," in *2010 IEEE International Symposium on Biomedical Imaging: From Nano to Macro*, 2010, pp. 872–875 [Online]. http://ieeexplore.ieee.org/xpls/abs_all.

[26] E. Konukoglu, W. M. Wells, S. Novellas, N. Ayache, R. Kikinis, P. M. Black, and K. M. Pohl, "Monitoring slowly evolving tumors," in *2008 5th IEEE International Symposium on Biomedical Imaging: From Nano to Macro*, 2008, pp. 812–815 [Online]. Available: http://ieeexplore.ieee.org/xpls/abs_all.jsp?arnumber=4541120.

[27] R. Gray, "Vector quantization," *IEEE ASSP Magazine*, vol. 1, no. 2, pp. 4–29, Apr. 1984 [Online]. http://ieeexplore.ieee.org/articleDetails.jsp?arnumber=1162229

[28] G. Pölzlbauer (2004) Survey and Comparison of Quality Measures for Self-Organizing Maps. *Proceedings of the Fifth Workshop on Data Analysis WDA'04*, pp. 67--82.

[29] D. N. Louis, A. Perry, G. Reifenberger, A. von Deimling, D. Figarella-Branger, W. K. Cavenee, H. Ohgaki, O. D. Wiestler, P. Kleihues, and D. W. Ellison, "The 2016 World Health Organization Classification of Tumors of the Central Nervous System: a summary," *Acta Neuropathol*, vol. 131, no. 6, pp. 803–820, May 2016 [Online]. Available: http://link.springer.com/article/10.1007/s00401-016-1545-1.

[30] M. Afshin, I. B. Ayed, A. Islam, A. Goela, T. M. Peters, and S. Li, "Global Assessment of Cardiac Function Using Image Statistics in MRI," in *Medical Image Computing and Computer-Assisted Intervention – MICCAI 2012: 15th International Conference, Nice, France, October 1-5, 2012, Proceedings, Part II*, N. Ayache, H. Delingette, P. Golland, and K. Mori, Eds. Berlin, Heidelberg: Springer Berlin Heidelberg, 2012, pp. 535–543 [Online]. Available at: http://dx.doi.org/10.1007/978-3-642-33418-4_66

[31] City of Las Vegas Economic and Urban Development Department and Redevelopment Agency. Demographics, 2013.

[32] Las Vegas Convention and Visitors Authority. Statistics, 2017.

[33] Singh, A. Review article: Digital change detection techniques using remotely-sense data. *Int. J. Remote Sens.* 10(6), 989–1003, 1989.

[34] Rosin, P.L., Ioannidis, E. Evaluation of global image thresholding for change detection. *Pattern Recognition Letters*. 24(14), 2345–2356, 2003.

[35] Otsu, N. A threshold selection method from gray-level histograms. *IEEE Trans. Syst. Man Cybern.* 9(1), 62–66, 1979.

[36] Kapur, J.N., Sahoo, P.K.,Wong, A.K.C. A new method for gray-level picture thresholding using the entropy of the histogram. *Comput. Vis. Graph. Image Process. 29(3)*, 273–285, 1984.

[37] Devore, J. *Probability and Statistics for Engineering and Science*. 6 edn. Thompson, 2004.

[38] Griffiths, G.H.Monitoring urban change from Landsat TM and Spot satellite imagery by image differencing. In: *Proceedings of the 1988 International Geoscience and Remote Sensing Symposium*, vol. 1, 1988.

[39] Saksa, T., Uuttera, J., Kolstrom, T., Lehikoinen,M., Pekkarinen, A., Sarvi, V. Clear-cut detection in boreal forest aided by remote sensing. Scandinavian J. *For. Res. 8(6)*, 537–546, 2003.

[40] Lu, D., Mausel, P., Batistella, M., Moran, E. Land-cover binary change detection methods for use in the moist tropical region of the Amazon: A comparative study. *Int. J. Remote Sens.* 26(1), 101–114, 2005.

[41] Malila,W.A. Change vector analysis: An approach for detecting forest changes with Landsat. In: *LARS Symposia*, p. 385, 1980.

[42] Johnson, R.D., Kasischke, E.S. Change vector analysis: A technique for the multispectral monitoring of land cover and condition. *Int. J. Remote Sens.* 19(3), 411–426, 1998.

[43] Klir, G.J., Yuan, B. *Fuzzy Sets and Fuzzy Logic Theory and Applications*. Prentice Hall, New York, 1995.

[44] Hays, J.; Efros, A. Im2GPS: estimating geographic information from a single image. In: *IEEE Conference on Computer Vision and Pattern Recognition*, 2008.

[45] Merril, K. R.; Jiajun, L. A comparison of four algorithms for change detection in an urban environment. *Remote Sensing of Environment*, 63, 95–100, 1998.

[46] NASA/Goddard Space Flight Center Landsat images obtained from USGS Earth Explorer. ID: 10721, Mar. 2012 [Online]. Available: http://svs.gsfc.nasa.gov/10721.

[47] Wieland, M.; Pittore, M. Performance Evaluation of Machine Learning Algorithms for Urban Pattern Recognition from Multi-spectral Satellite Images, *Remote Sensing*, vol. 6, no. 4, pp. 2912–2939, 2014.

[48] Schneider, C. A.; Rasband, W. S.; Eliceiri, K. W. NIH Image to ImageJ: 25 years of image analysis," *Nature Methods*, vol. 9, p. 671, 2012.

[49] Thévenaz, P.; Ruttimann, U.E.; Unser, M. A Pyramid Approach to Subpixel Registration Based on Intensity. *IEEE Transactions on Image Processing*, vol. 7, no. 1, pp. 27–41, 1998.

[50] Vettigli, G. *MiniSom*: *minimalistic and NumPy-based implementation of the Self Organizing Map*. https://github.com/JustGlowing/minisom

[51] Suzuki, K. Pixel-Based Machine Learning in Medical Imaging. International Journal of *Biomedical Imaging*, vol. 2012, pp. 1–18, 2012.

[52] K. M. Pohl, E. Konukoglu, S. Novellas, N. Ayache, A. Fedorov, I.-F. Talos, A. Golby, W. M. Wells, R. Kikinis, and P. M. Black (2011) A New Metric for Detecting Change in Slowly Evolving Brain Tumors: Validation in Meningioma Patients. *Operative Neurosurgery* http://content.wkhealth.com/linkback/openurl?sid=WKPTLP:landingpage&an=01787389-201103001-00030.

[53] Hartline, Haldan K., Henry G Wagner, Floyd Ratliff (1956). Inhibition in the eye of Limulus. The *Journal of General Psychology*. 5. 39, 651–671.

[54] Hebb, D. (1949) *The Organization of Behaviour*. John Wiley & Sons.

[55] Kayvan N, Rober S. (2012) *Biomedical Signal and Image processing*, 2nd edition. New York: CRC press.

[56] Rangayyan RM. (2001) *Biomedical signal analysis: a case study approach*. New York: Wiley-IEEE Press; 2001.

[57] Kacar S, Sakoglu Ü. (2016) Design of a novel biomedical signal processing and analysis tool for functional neuroimaging. *Comput Methods Programs Biomed* , 46–57.

[58] Sakoglu Ü, Calhoun VD. (2009) Temporal dynamics of functional network connectivity

at rest: a comparison of schizophrenia patients and healthy controls. *In: Proceedings of the 15th annual meeting of the organization for human brain mapping*. San Francisco.

[59] Case M, Zhang H, Mundhahl J, Datta Y, Nelson S, Gupta K, He B. (2017) Characterization of functional brain activity and connectivity using EEG and fMRI in patients with sickle cell disease. *Neuroimage: Clinical*, 14:1–17.

[60] Zhang CH, Lu Y, Brinkmann B, Welker K, Worrell G, He B. (2015) Lateralization and localization of epilepsy related hemodynamic foci using presurgical fMRI. *Clinical Neurophysiology*, 126:27–8.

[61] Darbari DS, Hampson JP, Ichesco E, Kadom N, Vezina G, Evangelou , Clauw DJ, Taylor Vi JG, Harris RE. (2015) Frequency of hospitalizations for pain and association with altered brain network connectivity in sickle cell disease. *J Pain*, 16:1077–86.

[62] Lamata P, Casero R, Carapella V, Niederer SA, Bishop MJ, Schneider JE, Kohl P, Grau V. (2015) Images as drivers of progress in cardiac computational modelling. *Prog Biophys Mol Biol*, 115:198–212.

[63] Zidan SH, Shetata SM. (2016) Value of multi-detector computed tomography in delineation of the normal cardiac conduction system and related anatomic structures. *Egypt J Radiol Nuclear Med*, 14:1333–47.

[64] Hemalatha R, Santhiyakumari N, Madheswaran M, Suresh S. (2016) Segmentation of 2D and 3D images of carotid artery on unified technology learning platform. *Procedia Technology*, 25:12–9, Global Colloquium on Recent Advancement and Effectual Researches in Engineering, Science and Technology (RAEREST 2016).

[65] Kasehagen B, Ellis R, Mawston G, Allen S, Hing W. (2016) Assessing the reliability of ultrasound imaging to examine radial nerve excursion. *Ultrasound Med Biol*, 42(7):1651–9.

[66] Yu J, Wang Y, Chen P, Shen Y. Fetal (2008) Abdominal contour extraction and measurement in ultrasound images. *Ultrasound Med Biol*, 34(2):169–82.

[67] Hadjerci O, Hafiane A, Conte D, Makris P, Vieyres P, Delbos A. (2016) Computer-aided detection system for nerve identification using ultrasound images: a comparative study. *Inform Med Unlocked*, 3:29–43.

[68] Ciaccio EJ, Biviano AB, Iyer V, Garan H. (2017) Trends in quantitative methods used for atrial fibrillation and ventricular tachycardia analyses. *Inform Med Unlocked*, 6:12–27.

[69] Chou C-P, Peng N-J, Chang T-H, Yang T-L, Hu C, Lin H-S, Huang J-S, Pan H-B. (2015) Clinical roles of breast 3T MRI, FDG PET/CT, and breast ultrasound for asymptomatic women with an abnormal screening mammogram. *J Chin Med Asso*, 78: 719–25.

[70] Aswathy MA, Jagannath M. (2016) Detection of breast cancer on digital histopathology images: Present status and future possibilities. *Informatics in Medicine Unlocked*. Available online 11 November 2016.

[71] Nguyen H, Stelling A, Kuramoto A, Patel C, Keller J. (2014) Malignant rhabdoid tumor of the liver: Findings at US, CT, and MRI, with histopathologic correlation. *Radiol Case Rep* 9(1):1–3.

[72] Gutiérrez-Gnecchi JA, Morfin-Magaˆna R, Lorias-Espinoza R. Tellez-Anguiano Ac, Reyes-Archundia E, Méndez-Patino A, Aneda-Miranda RC (2017) DSP-based arrhythmia classification using wavelet transform and probabilistic neural network. *Biomed Signal Process Control*, 32:44–56.

[73] Okada M. (1979) A digital filter for the QRS complex detection. *IEEE Trans Bio-Med Eng BME,* 26:700–3.

[74] Kadambe S, Murray R, Boudreaux-Bartels GF. (1999) Wavelet transform-based QRS complex detector. *IEEE Trans Biomed Eng*, 46:838–48.

[75] He B, Li G, Lian J. (2002) A spline Laplacian ECG estimator in realistic geometry volume conductor. *IEEE Trans Biomed Eng*, 49(2):110–7.

[76] Perrin F, Pernier J, Bertrand O, Giard MH, Echallier JF. (1987) Mapping of scalp potentials by surface spline interpolation. *Electroencephalogr Clin Neurophysiol*, 66:75–81.

[77] He B. (1999) Brain electrical source imaging: Scalp Laplacian mapping and cortical imaging. *Crit Rev Biomed Eng*, 27:149–88.

 doi:10.20944/preprints201710.0166.v2

[78] Jero SE, Ramu P. (2016) Curvelet-based ECG steganography for data security. *Electron. Lett.,* 52(4):283–5.

[79] Starck J-L, Candès EJ, Donoho DL. (2002) The curvelet transform for image denoising. *IEEE Trans Image Process*, 11(6):670–84.

[80] Sahoo D, Biswal P, Das T, Sabut S. (2016) De-noising of ECG signal and QRS detection using Hilbert transform and adaptive thresholding. *Procedia Technol*, 25:68–75, Global Colloquium in Recent Advancement and Effectual Researches in engineering, Science and Technology (RAEREST).

[81] Annavarapu A, Kora P. (2016) ECG-based atrial fibrillation detection using different orderings of conjugate symmetric-complex Hadamard transform. *Int J Cardiovasc Acad,* 2:151–4.

[82] Kazemi S, Ghorbani A, Amindavar H, Morgan DR. (2016) Vital-sign extraction using bootstrap based generalized wavelet transform in heart and respiration monitoring radar system. *IEEE Trans Instrum Meas*, 65(2):255–63.

[83] Bian Y, LI H, Zhao L, Yang G, Geng L. (2011) Research on steady state visual evoked potentials based on wavelet packet technology for brain-computer interface. *Adv Control Eng Inform Sci Procedia Eng*, 15:2629–63.

[84] Guanyyu BIN, Jing ZY, Rong GX. (2008) Steady state visual evoked potential measurement using a phase-locking method. *J Tsinghua Univ Sci Technol*, 48(9):127–

[85] Zhao L, Yuan P, Xian L. (2010) Research on SSVEP feature extraction based on HHT. *Conference Proceedings on Fuzzy Systems and Knowledge*, 2220–3.

[86] Amorim P, Moraes T, Fazanaro D, Silva J, Pedrini H. (2017) Electroencephalogram signal classification based on shearlet and contourlet transforms. *Exp Syst Appl*, 67:140–7.

[87] Patidar S, Panigrahi T. (2017) Detection of epileptic seizure using Kraskov entropy applied on tunable-Q wavelet transform of EEG signals. *Biomed Signal Process Control,* 34:74–80.

[88] Kawakatsu H. (2015) Methods for Evaluating Pictures and Extracting Music by 2D DFA and 2D FFT. In: Proceedings of the 19th international conference on knowledge based and intelligent information and engineering systems. *Procedia Computer Science,* 60:834–40.

[89] Kawakatsu, H. Fluctuation analysis for photographs of tourist spots and music extraction from photographs (2014) *Lecture Notes in Engineering and Computer Science. In: Proceedings of the World Congress on Engineering* WCE 2014: 1558–612. July, London, UK.

[90] Bhateja V, Patel H, Krishn A, Sahu A, Lay-Ekualille A. (2015) Multimodal medical image sensor fusion framework using cascade of wavelet and contourlet transform domains. *IEEE Sensors Journal*, 15(12):6783–90.

[91] Mjahad A, Rosado-Muñoz A, Bataller-Mompeán M, Francés-Víllora JV, Guerrero-Martínez JF. (2017) Ventricular Fibrillation and Tachycardia detection from surface ECG using time-frequency representation images as input dataset for machine learning. *Comput Methods Programs Biomed*, 141:119–27.

[92] Arenja N, Riffel JH, Djioko CJ, Andre F, Fritz T, Halder M, Zelniker T, Kristen AV, Korosoglou G, Katus HA, Buss SJ. (2016) Right ventricular long axis strain-validation of a novel parameter in non-ischemic dilated cardiomyopathy using standard cardiac magnetic resonance imaging. *Eur J Radiol*, 85:1322–8.

[93] Mavratzakis A, Herbert C, Walla P. (2016) Emotional facial expressions evoke faster orienting responses, but weaker emotional responses at neural and behavioural levels compared to scenes: a simultaneous EEG and facial EMG study. *NeuroImage*, 124: 931–46.

[94] Vuilleumier P, Pourtois G. (2007) Distributed and interactive brain mechanisms during emotion face perception: evidence from functional neuroimaging. *Neuropsychologia,* 45(1):174–94.

[95] Olofsson JK, Nordin S, Sequeira H, Polich J. (2008) Affective picture processing: an integrative review of ERP findings. *Biol Psychol*, 77(3):247–65.

[96] Vulliemoz S, Rodionov R, Carmichael DW, Thornton R, Guye M, Lhatoo SD, Michel CM, Duncan JS, Lemieux L. (2010) Continuous EEG source imaging enhances analysis of EEG-fMRI in focal epilepsy. *NeuroImage,* 49:3219–29.

[97] Hinterberger T, Weiskopf N, Veit R, Wilhelm B, Betta E, Birbaumer N. (2004) An EEG-driven brain-computer interface combined with functional magnetic resonance imaging (fMRI). *IEEE Trans Biomed Eng*, 51(6):971–4.

[98] Cagnie B, Dirks R, Schouten M, Parlevliet T, Cambier D, Danneels D. (2011) Functional reorganization of cervical flexor activity because of induced muscle pain evaluated by muscle functional magnetic resonance imaging. *Manual Ther*, 16:470–5.

[99] Metz CE. (2006) Receiver operating characteristic (ROC) analysis: a tool for quantitative evaluation of observer performance and imaging systems. *JACR. 2006*,3:413–22

[100] Wagner RF, Metz CE, Campbell G. (2007) Assessment of medical imaging systems and computer aids: a tutorial review. *Acad Radiol,* 14:723–48.

[101] Gur D. (2007) Objectively measuring and comparing performance levels of diagnostic imaging systems and practices (editorial). *Acad Radiol*, 14:641–2.

[102] Burns, G.S. and Joyce, A.T. (1981). Evaluation of land cover change detection techniques using Landsat MSS data. *Proc. 7th Pecora Symposium*, Sioux Falls, South Dakota, USA, pp. 252-260.

[103] Caselles, V. and Lopez Garcia, M.J. (1989). An alternative simple approach to estimate atmospheric correction in multitemporal studies. *Int. J. Remote Sens.*, 10: 1127-1134.

[104] Conel, J.E. (1990). Determination of surface reflectance and estimates of atmospheric optical depth and single scattering *albedo* from the Landsat Thematic Mapper data. *Int. J. Remote Sens.*, 11: 783-828.

[105] Coppin, P.R. and Bauer M.E. (1994). Processing of multitemporal Landsat TM imagery to optimize extraction of forest cover change features. *IEEE Trans. Geosci. Remote Sens.*, 32: 918-927.

[106] Coppin, P. R. and Bauer M. E. (1996). Digital change detection in forest ecosytems with remote sensing imagery. *Remote Sensing Reviews*, Vol. 13, pp. 207-234, Netherlands: Amsterdam B.V.

[107] Du, Y., Cihlar, J., Beaubien, J. and Latifovic, R. (2001). Radiometric normalization, compositing and quality control for satellite high resolution image mosaics over large areas. *IEEE Trans. Geosci. Remote Sens.,* 39(3): 623-634.

[108] Fraser, R.S., Ferrare, R.A., Kaufmann, Y.J., and Mattoo, S. (1989). Algorithm for atmospheric corrections of aircraft and satellite imagery. *NASA Technical Memorandum 100751*, 1-106.

[109] Guindon, B. (1997). Assessing the radiometric fidelity of high resolution satellite image mosaics. *ISPRS Journal of Photogrammetry & Remote Sens.*, 52(2): 229-243.

[110] Hall, F.G., Strebel, D.E., Nickeson, J.E. and Goetz, S.J. (1991). Radiometric rectification: Toward a common radiometric response among multi-data, multi-sensor images. *Remote Sensing Environ.,* 35: 11-27.

[111] Heo, J and Fitzhugh, F.W. (2000). A standardized radiometric normalization method for change detection using remotely sensed imagery. *ISPRS Journal of Photogrammetry & Remote Sens.*, 60: 173-181.

[112] Kaufman, Y. J. (1988). Atmospheric effect on spectral signature. *IEEE Trans. Geosci. Remote Sens.,* 26(4): 441-451.

[113] Kneizys, F.X., Shettle, E.P., Gallery, W.O., Chetwynd, J.H., Abreu, L.W., Selby, J.E.A., Clough, S.A., and Fenn, R.W. (1983). Atmospheric transmittance /radiance: computer code LOWTRAN-6, AFGL-TR-83-0187. *Air Force Geophysics Lab*, Hanscom AFB, Massachusetts.

[114] Celik, T. (2009) Unsupervised change detection in satellite images using principal component analysis and k-means clustering. *IEEE Geoscience and Remote Sensing Letters*, 6(4) ,772-776.

[115] Neagoe, V.E., Neghina, M., and Datcu, M. (2012). Neural network techniques for automated landcover change detection in multispectral satellite time series imagery", *In International Journal of Mathematical Models and Methods in Applied Science.* Issue. 1, Vol. 6, pp.130-139.

 doi:10.20944/preprints201710.0166.v2

[116] Patra, S., Ghosh, S., and Ghosh, A., (2007). Unsupervised Change Detection in Remote-Sensing Images using Modified Self-Organizing Feature Map Neural Network, *In IEEE Proceedings of the International Conference on Computing: Theory and Applications*, ICCTA'07.

[117] Neagoe, V.E., Stoica, R.M., and Ciurea, A.I. (2012) Concurrent Self-Organizing Maps for Change Detection in Time Series of Multispectral Remote Sensing Imagery? *In Recent Advances in Information Science*, ISBN: 978-1-61804-140-1.

[118] Ghosha, S., Roya, M., Ghoshb, A. (2014) Semi-supervised change detection using modified self-organizing feature map neural network. *Applied Soft Computing*, Vol. 15, pp.1–20.

[119] Stefanovič, P., Kurasova, O. (2014). "Investigation on Learning Parameters of Self-Organizing Maps", In *Baltic J. Modern Computing,* Vol. 2, No. 2, pp.45-55.

[120] Breard, G. T., (2017). Evaluating Self-Organizing Map Quality Measures as Convergence Criteria. University of Rhode Island Open Access Master's Theses. Paper 1033.

[121] Torres-Huitzil, C., Popovych, O., Girau, B. (2017) Fault -tolerance of Self-Organizing Maps. Available online: https://hal.inria.fr/hal-01574212/document